AGU PUBLICATIONS

JGR

Journal of Geophysical Research: Atmospheres

RESEARCH ARTICLE
10.1002/2015JD023926

Key Points:
- We examine future tropospheric O_3 in China driven by emission change under RCPs
- RCP6.0 is the worst scenario for O_3 air quality in China over 2040-2050
- RCP2.6 is a significantly improving scenario for both air quality and climate

Supporting Information:
- Figures S1–S4

Correspondence to:
H. Liao,
hongliao@mail.iap.ac.cn

Citation:
Zhu, J., and H. Liao (2016), Future ozone air quality and radiative forcing over China owing to future changes in emissions under the Representative Concentration Pathways (RCPs), *J. Geophys. Res. Atmos.*, *121*, 1978–2001, doi:10.1002/2015JD023926.

Received 12 JUL 2015
Accepted 25 JAN 2016
Accepted article online 28 JAN 2016
Published online 26 FEB 2016

Future ozone air quality and radiative forcing over China owing to future changes in emissions under the Representative Concentration Pathways (RCPs)

Jia Zhu[1,2] and Hong Liao[1]

[1]State Key Laboratory of Atmospheric Boundary Layer Physics and Atmospheric Chemistry, Institute of Atmospheric Physics, Chinese Academy of Sciences, Beijing, China, [2]University of Chinese Academy of Sciences, Beijing, China

Abstract We apply the nested grid version of the Goddard Earth Observing System (GEOS) chemical transport model (GEOS-Chem) to assess 2000–2050 changes in O_3 air quality and associated radiative forcing in China owing to future changes in emissions under the Representative Concentration Pathways (RCP2.6, RCP4.5, RCP6.0, and RCP8.5). Changes in surface layer O_3 concentrations, numbers of O_3 exceedance days (days with maximum daily 8 h average (MDA8) O_3 exceeding 74.7 ppbv), and tropospheric O_3 radiative forcing (RF) are simulated for 2000–2050. Over China, RCP8.5 is the worst scenario for near future (2020–2030) and RCP6.0 is the worst scenario over 2040–2050; the maximum increases in annual mean surface layer O_3 concentrations of 6–12 ppbv relative to present day (year 2000) are found over southern China in 2020 and 2030 under RCP8.5 and in 2040 and 2050 under RCP6.0. The numbers of MDA8 O_3 exceedance days are simulated to be 10, 0, 0, and 2 days over Beijing-Tianjin-Tanggu (BTT), Yangtze River Delta (YRD), Pearl River Delta (PRD), and Sichuan Basin (SCB), respectively, in the present day (year 2000). No exceedance days are simulated in year 2050 for all the four regions under RCP2.6 and RCP4.5, but extremely high numbers of exceedance days are found in 2050 under RCP6.0 (with 102, 75, 57, and 179 days in BTT, YRD, PRD, and SCB, respectively) and in 2030 under RCP8.5 (with 94, 60, 34, and 162 days in BTT, YRD, PRD, and SCB, respectively). The tropospheric O_3 RF in 2050 relative to 2000 averaged over eastern China (18°–45°N, 95°–125°E) is simulated to be −0.11, 0.0, 0.01, and 0.14 W m^{-2} under RCP2.6, RCP4.5, RCP6.0, and RCP8.5, respectively. When we consider both the health and climate impacts of tropospheric O_3 over China in 2050, RCP2.6 is a significantly improving scenario for both air quality and climate, RCP4.5 is a significantly improving scenario for air quality but has small consequences for climate, RCP6.0 is a significantly worsening scenario for air quality and a slightly worsening scenario for climate, and RCP8.5 is a slightly worsening scenario for air quality and a significantly worsening scenario for climate. These results indicate that to simultaneously abate air pollution and climate warming induced by O_3 in China, both the anthropogenic emissions of NO_x, CO, nonmethane volatile organic compounds (NMVOCs), and global CH_4 levels should be reduced, as represented by RCP2.6.

1. Introduction

Tropospheric O_3 is a secondary pollutant produced during the photochemical oxidation of nitrogen oxides (NO_x), carbon monoxide (CO), methane (CH_4), and nonmethane volatile organic compounds (NMVOCs). Tropospheric O_3 has an adverse effect on human health [*Fann et al.*, 2012; *Yang et al.*, 2012; *Jhun et al.*, 2014], ecosystems [*Fuentes et al.*, 2013; *Yue and Unger*, 2014], and crops [*Feng and Kobayashi*, 2009; *Wilkinson et al.*, 2011; *Tai et al.*, 2014] and also contributes to global warming as an important greenhouse gas [*Intergovernmental Panel on Climate Change* (*IPCC*), 2013]. High O_3 concentrations have been observed in many Chinese sites, with seasonal mean concentrations of 20–60 ppbv [*Zhu et al.*, 2006; *Wang et al.*, 2009, 2011; *Tang et al.*, 2013; *Zhang et al.*, 2014] and episodic concentrations of exceeding 100 ppbv [*Zhu et al.*, 2004; *Wang et al.*, 2008, 2010; *Lam et al.*, 2013; *Tang et al.*, 2013]. It is of interest to project future O_3 levels over China in response to changes in emissions in the coming decades.

Earlier studies to project future O_3 concentrations generally used the Intergovernmental Panel on Climate Change (IPCC) Special Report on Emissions Scenarios (SRES) that were designed for the IPCC Fourth Assessment Report [*Jacob and Winner*, 2009]. More recently, a new set of emissions, Representative Concentration Pathways (RCPs), has been developed for the Fifth Coupled Model Intercomparison Project (CMIP5) simulations [*Moss et al.*, 2010; *Taylor et al.*, 2012] in support of the IPCC Fifth Assessment Report. The RCPs consist of four scenarios (RCP2.6, RCP4.5, RCP6.0, and RCP8.5) spanning 2000–2100, which are

Table 1. Comparisons of Impacts on Surface O_3 Concentrations (or Tropospheric O_3 Burden and Radiative Forcing) by Future Changes in Anthropogenic Emissions With Those by Future Changes in Climate

					Absolute or Percentage Changes[a]		
Reference	Domain	Model Year	Scenario	Parameter	Climate[b]	Emission[b]	Combined Climate and Emission[b]
Stevenson et al. [2013]	Global	2030 relative to 1850	RCP8.5	Global tropospheric O_3 radiative forcing (m W m^{-2})	−25	NA	439
		2100 relative to 1850			−33		582
Wu et al. [2008a]	Global	2000–2050 Annual	SRES A1B	Global tropospheric O_3 burden (%)	+1.6	+17	+18
Tagaris et al. [2007]	West U.S.	2000–2050 JJA[c]	SRES A1B	MDA8[d] surface O_3 concentrations (%)	+0.9	NA	−11.6
	Plains U.S.				−0.1		−15.8
	Midwest U.S.				−2.5		−24.4
	Northeast U.S.				+2.8		−20.2
	Southeast U.S.				+0.3		−27.9
	U.S.				0.0		−18.9
Racherla and Adams [2009]	U.S.	1990–2050 JJA	SRES A2	MDA8 surface O_3 concentrations (ppbv)	+0.5	+9.1	NA
Lauwaet et al. [2014]	Belgium	2000–2030 Annual	RCP4.5	Annual mean surface O_3 concentrations (%)	−3	NA	+23
Wang et al. [2013]	China	2000–2050 Summer	SRES A1B	Afternoon surface O_3 concentrations (ppbv)	+0.4	+11.6	+11.9
Lee et al. [2015]	30°–40°N, 110°–123°E	2000–2050 Summer	SRES A2	MDA8 surface O_3 concentrations (ppbv)	−2.2	+12.1	+11.7[e]
Liu et al. [2013]	Pearl River Delta	2000–2050 Autumn	SRES A1B	Afternoon surface O_3 concentrations (ppbv)	+1.5	+6.1[f]	+11.4

[a]The absolute or percentage changes are averaged over the domains shown in the second column.
[b]Climate, emission, and combined climate and emission indicate the effects on O_3 by climate change alone, emission change alone, and the combined changes in climate and emissions, respectively. NA: not available.
[c]JJA indicates June-July-August.
[d]MDA8 O_3 indicates maximum daily 8 h average O_3.
[e]The combined changes in regional climate, lateral chemical boundary conditions, and emissions.
[f]The effect of emissions does not include the impact of increases in CH_4, which would lead to even larger increases in O_3 concentration over the Pearl River Delta.

named according to the approximate values of the radiative forcing (in W m^{-2}) in 2100 relative to the preindustrial times. The RCP4.5 scenario, for example, leads to a global radiative forcing of 4.5 W m^{-2} by 2100.

Future concentrations of tropospheric O_3 are influenced by future changes in anthropogenic emissions [*Racherla and Adams*, 2009; *Butler et al.*, 2012; *Wild et al.*, 2012; *Xie et al.*, 2013; *Lapina et al.*, 2015] and climate [*Racherla and Adams*, 2006; *Wu et al.*, 2008a, 2008b; *Katragkou et al.*, 2011; *Juda-Rezler et al.*, 2012; *Langner et al.*, 2012; *Val Martin et al.*, 2015]. A warmer climate is predicted to reduce tropospheric O_3 in remote regions by higher temperature and water vapor [*Brasseur et al.*, 2006; *Liao et al.*, 2006; *Murazaki and Hess*, 2006; *Fiore et al.*, 2012] but to increase O_3 levels over populated areas as a result of slower transport, enhanced biogenic hydrocarbon emissions, and decomposition of peroxyacetyl nitrate at higher temperature [*Katragkou et al.*, 2011; *Rasmussen et al.*, 2012; *Doherty et al.*, 2013; *Mao et al.*, 2013; *Kim et al.*, 2014]. Table 1 lists the previous modeling studies that have compared the impact on O_3 by future changes in emissions with that by future changes in climate. By using Goddard Earth Observing System (GEOS) chemical transport model (GEOS-Chem) driven by meteorological fields from NASA/Goddard Institute for Space Studies general circulation model (NASA/GISS GCM), *Wu et al.* [2008a] found that the global tropospheric O_3 burden would change by +1.6%, +17%, and +18% over 2000–2050 owing to climate change alone, emission change alone, and the combined changes in climate and emissions, respectively, under the SRES A1B scenario. By using the same NASA GISS GCM/GEOS-Chem model combination as in *Wu et al.* [2008a], *Wang et al.* [2013] reported that summer afternoon-mean surface layer O_3 concentrations averaged over China would increase by 0.4 ppbv, 11.6 ppbv, and 11.9 ppbv over 2000–2050 due to climate change alone, emission change alone, and the combined changes in climate and emissions, respectively, under the SRES A1B scenario. By using the MM5/CMAQ model combination with 54 km horizontal resolution, *Lee et al.* [2015] reported that summertime surface layer maximum daily 8 h average (MDA8) O_3 concentrations averaged over the polluted region (30°–40°N, 110°–123°E) of China would change over 2000–2050 by −2.2 ppbv, +3.3 ppbv, +12.1 ppbv,

and +11.7 ppbv owing to regional climate change alone, changes in lateral chemical boundary conditions alone, emission change alone, and the combined changes, respectively, under the SRES A2 scenario. The studies listed in Table 1 have shown that the impact of future climate change on tropospheric O_3 is much smaller than the impact of future changes in emissions, especially over polluted regions of China (e.g., eastern and central China).

A number of global modeling studies have projected future changes in global tropospheric O_3 under the new RCP scenarios [*Kawase et al*., 2011; *Eyring et al*., 2013; *Szopa et al*., 2013; *Young et al*., 2013a; *Kim et al*., 2014; *Val Martin et al*., 2015]. However, these global modeling studies were conducted at coarse spatial resolutions, which often lacked detailed information on regional and local changes. Besides, the use of coarsely resolved global models with a highly resolved gridded emission field (e.g., 0.5° × 0.5° for RCP emissions; see section 2.2) led to biases due to the instantaneous dilution of the emissions into the model grid cells [*Butler et al*., 2012]. High-resolution regional models have been used to project O_3 changes over America [*Kelly et al*., 2012; *Gao et al*., 2013; *Pfister et al*., 2014] and Europe [*Coleman et al*., 2013]. *Gao et al*. [2013] simulated 2000–2050 changes in O_3 in the United States under RCP4.5 and RCP8.5, by using the WRF and CMAQ models. Their results showed that surface O_3 concentrations in summer during 2057–2059 would decrease by 6–10 ppbv compared to the present day (2001–2004) under RCP4.5 mainly due to the large reductions in emissions of O_3 precursors. However, under RCP8.5, the simulated surface O_3 levels would increase by 3–10 ppbv in winter across nearly the entire continental United States mainly owing to the increased methane. By using a nested regional climate model with chemistry (NRCM-Chem), *Pfister et al*. [2014] reported that the 5th–95th percentile range for summertime MDA8 surface O_3 over the United States would reduce from 31–79 ppbv to 27–55 ppbv under the RCP8.5 emission and SRES A2 climate scenarios from 2000 to 2050. *Coleman et al*. [2013] reported that the average O_3 concentrations would reduce by 2.0 ppb over domains encompassing Europe and the northeast Atlantic between 2006 and 2100 under the RCP6.0 scenario with the most significant decrease occurring after 2050 due to the pattern in changing emissions.

These existing regional studies on future projection of tropospheric O_3 under the RCPs were focused on American and European countries, and they only paid attention to the changes in surface layer concentrations from the perspective of air quality. In addition, due to the limited computational resources, these regional modeling studies were focused on future O_3 in 2030 or 2050 under one or two RCP scenarios. We present here a study to quantify future changes in seasonal and annual mean surface layer O_3 concentrations, MDA8 O_3 exceedance days, as well as tropospheric O_3 radiative forcing in China over 2000–2050 for every decade under the four RCPs as a result of the future changes in anthropogenic emissions. We do not include any changes in climate, which would also impact future ozone levels, especially on relatively clean areas, but focus on the effects of anthropogenic precursor emission changes alone over polluted regions in China. We use the nested grid version of the GEOS-Chem model with a horizontal resolution of 0.5° latitude × 0.667° longitude, which is close to the resolution of 0.5° × 0.5° of RCP emissions. We pay special attention to future changes in O_3 over the four heavily polluted regions in China, including Beijing-Tianjin-Tanggu (BTT, 35°–40°N, 114°–120°E), Yangtze River Delta (YRD, 29°–33°N, 118°–122°E), Pearl River Delta (PRD, 21°–24°N, 112°–116°E), and Sichuan Basin (SCB, 28°–32°N, 102°–108°E).

The descriptions of model, emissions, and numerical simulations are presented in section 2. Simulated present-day O_3 levels are presented and evaluated in section 3. Section 4 examines projected changes in OH concentrations over China under the RCP scenarios. The projected future changes in O_3 air quality and radiative forcing in China are presented in sections 5 and 6, respectively.

2. Model Description, Emissions, and Numerical Experiments

2.1. GEOS-Chem Model

The simulations of tropospheric O_3 are carried out with the nested grid capability of the GEOS-Chem model with a horizontal resolution of 0.5° latitude by 0.667° longitude (version 9.1.3, http://acmg.seas.harvard.edu/geos/), driven by the assimilated year 2010 GEOS-5 meteorological data from the Goddard Earth Observing System (GEOS) of the NASA Global Modeling Assimilation Office (GMAO). The nested domain is set over Asia (70°–150°E, 11°S–55°N). The high-resolution regional simulation is coupled to the low-resolution global GEOS-Chem simulation through lateral boundary conditions of tracer concentrations that are updated every 3 h [*Chen et al*., 2009].

The GEOS-Chem model includes coupled O_3-NO_x-hydrocarbon chemistry (~80 species and ~300 chemical reactions) [*Bey et al*., 2001] and aerosols including $SO_4^{2-}/NO_3^-/NH_4^+$ [*Park et al*., 2004; *Pye et al*., 2009], BC and OC [*Park et al*., 2003], mineral dust [*Fairlie et al*., 2007], and sea salt [*Alexander et al*., 2005]. The simulations account for the impacts of aerosols on distributions and concentrations of O_3 through heterogeneous reactions and changes in photolysis rates [*Lou et al*., 2014]. The cross-tropopause O_3 flux is represented by the synthetic O_3 (Synoz) method [*McLinden et al*., 2000], which imposes a global annual cross-tropopause O_3 flux of 500 Tg yr^{-1}.

2.2. Emissions

Global anthropogenic emissions of O_3 precursors, aerosol precursors, and aerosols (NO_x, CO, NMVOCs, SO_2, NH_3, BC, and OC) for every decade over 2000–2050 under RCP2.6, RCP4.5, RCP6.0, and RCP8.5 are downloaded from the website http://www.iiasa.ac.at/web-apps/tnt/RcpDb. The RCP concentrations for CH_4 are also available from this website. The gridded $0.5° \times 0.5°$ emissions include 12 sectors (surface transportation, shipping, aviation, energy production and distribution, solvents, waste management and disposal, industrial combustion, residential and commercial fuel use, agriculture (animals, rice, and soil), agricultural waste burning, grassland burning, and forest burning). The NMVOC species in the RCP emission inventories are mapped to the species in the GEOS-Chem model as described in http://acmg.seas.harvard.edu/geos/wiki_docs/emissions/GEOS-Chem_RCP_emissions.pdf.

In the RCP inventories, emissions from shipping, aviation, and biomass burning have monthly variations. However, seasonal variations are not available for other anthropogenic sectors. We obtain monthly scaling factors for O_3 precursors, aerosol precursors, and aerosols from EDGAR for the project of the TF HTAP V2 of year 2010 (http://edgar.jrc.ec.europa.eu/htap_v2/index.php?SECURE=123) and apply these gridded monthly scaling factors to the RCP anthropogenic emissions for all years and all RCPs. The HTAP_V2 emissions over China domain are from Multi-resolution Emission Inventory for China (MEIC) database [*He*, 2012], which was developed by Tsinghua University, China, by continuously updating and improving the emission databases [*Zhang et al*., 2007, 2009; *Lei et al*., 2011]. The residential sector contributes largely to CO emissions in China, which are the highest in winter due to the residential heating needs. The transportation and industrial sectors are the major sources of NO_x in China, which have weak seasonal variations throughout the year. The ratios of monthly CO, NMVOCs, and NO_x emissions between maxima and minima in China are 1.8, 1.5, and 1.4, respectively, which are close to the values of 1.6 and 1.3 for CO and NO_x reported in the study of *Zhang et al*. [2009].

The projected annual anthropogenic emissions of NO_x, CO, and NMVOCs over China from 2000 to 2050 for every decade under the four RCPs are shown in Figures 1a–1c. The total anthropogenic emissions of NO_x, CO, and NMVOCs in China in 2000 are estimated to be 3.6 Tg N yr^{-1}, 124.2 Tg CO yr^{-1}, and 5.6 Tg C yr^{-1}, respectively. For a given scenario, anthropogenic emissions of NO_x, CO, and NMVOCs follow a similar pattern over 2000–2050. Under RCP2.6, the emissions of these species increase from 2000 to 2010 (or 2020), and then decrease sharply to 2050, leading to the decreases of 35.9%, 49.3%, and 41.7% from 2000 to 2050 for NO_x, CO, and NMVOCs, respectively. Under RCP4.5, all Chinese emissions have peaks at 2020 and then decrease to 2050. The similar temporal evolutions of anthropogenic emissions under RCP2.6 and RCP4.5 lead to very close emission values in 2050. For RCP6.0, Chinese emissions increase continuously from 2000 to 2050 for all species, with significant increases of 112.2%, 113.0%, and 121.4% in emissions of NO_x, CO, and NMVOCs, respectively, from 2000 to 2050. It is noted that although the RCP6.0 scenario seems to be unmitigated over 2000–2050 over China, emissions decrease sharply after 2050 as one would expect [*IPCC*, 2013]. The RCP8.5 has peaks at 2020 for NO_x and CO and at 2030 for NMVOCs. NO_x emissions increase sharply by 131.3% from 2000 to 2020 under RCP8.5.

Figure 1d shows the pathways for the global CH_4 abundance used in our simulations of O_3. The four scenarios indicate a wide range of possible CH_4 mixing ratios. The CH_4 mixing ratio in 2000 is 1751 ppb, which is projected to decrease by 17.1% under RCP2.6 and increase by 56.5% under RCP8.5 in 2050. The RCP4.5 and RCP6.0 have slight increases in CH_4 by 2050.

Natural emissions of O_3 precursors, including biogenic NMVOCs and NO_x from lighting and soil, are calculated based on the GEOS-5 meteorological parameters. Biogenic NMVOC emissions are calculated using the module of Model of Emissions of Gases and Aerosols from Nature [*Guenther et al*., 2006]. Lightning NO_x emissions are described by *Sauvage et al*. [2007] and *Murray et al*. [2012]. Soil NO_x emissions are

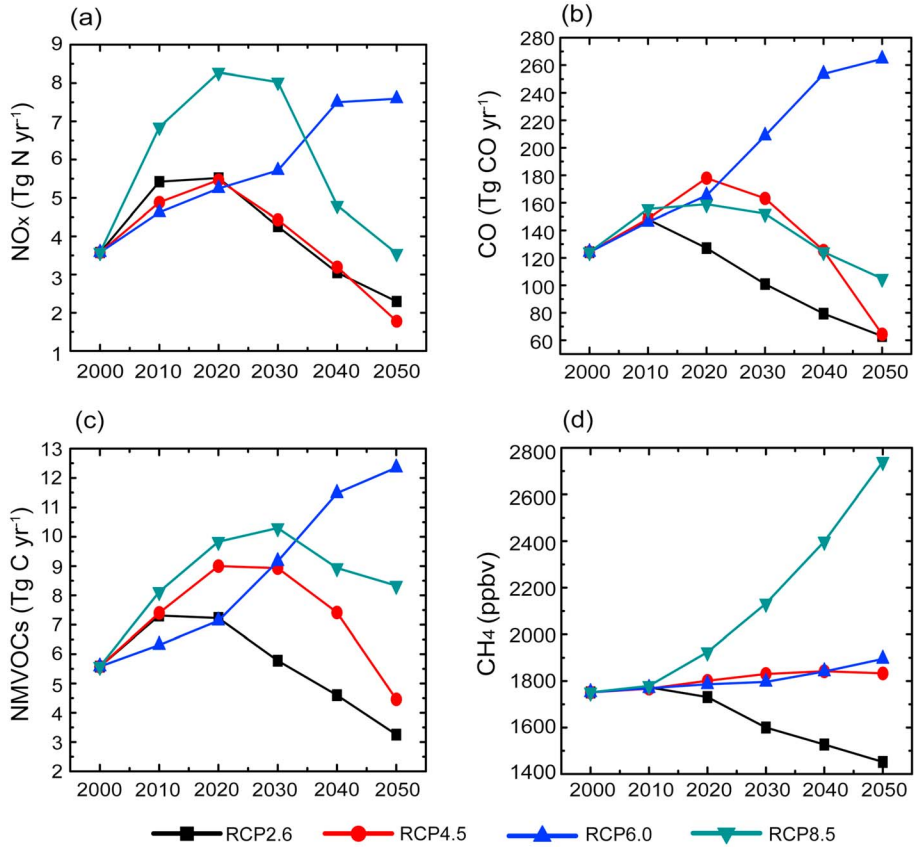

Figure 1. Evolutions of annual anthropogenic emissions over 2000–2050 in China under the four RCPs for (a) NO_x (Tg N yr^{-1}), (b) CO (Tg CO yr^{-1}), and (c) NMVOCs (Tg C yr^{-1}). (d) Evolution of global CH_4 abundance (ppb) over 2000–2050 under the four RCPs.

calculated using the algorithm proposed by *Yienger and Levy* [1995]. Biogenic emissions of NMVOCs, lightning NO_x emissions, and soil NO_x emissions over China are calculated to be 18.07 Tg C yr^{-1}, 0.30 Tg N yr^{-1}, and 0.26 Tg N yr^{-1}, respectively, on the basis of the GEOS-5 meteorological parameters for year 2010.

2.3. Numerical Simulations

Figure 2 shows the schematic overview of numerical experiments. We perform simulations of O_3 with present-day emissions (year 2000) and future emissions (years 2010, 2020, 2030, 2040, and 2050) for each of the four RCPs. All simulations are driven by the assimilated GEOS-5 meteorological fields for year 2010. Each simulation is carried out for 18 months with the first 6 months treated as model spin-up for both low-resolution (4° latitude by 5° longitude) global simulations that provide boundary conditions and the nested high-resolution (0.5° latitude by 0.667° longitude) simulations. The global simulations thus provide consistent lateral boundary conditions of tracer concentrations for the nested simulations every 3 h. We present annual or seasonal mean O_3 concentrations, MDA8 O_3 concentrations, and radiative forcing by tropospheric O_3 in the subsequent sections.

3. Simulated Present-Day O_3 Levels Over China and Model Evaluation

3.1. Seasonal Mean Surface Layer O_3 Concentrations

Figure 3 shows the simulated seasonal mean surface layer O_3 concentrations for present day (year 2000). Over eastern China, concentrations of O_3 in northern China are the highest in June-July-August (JJA) due to the strong photochemistry and lowest in December-January-February (DJF) because of the weak sunlight. In southern China, however, simulated O_3 levels are the lowest in JJA, because the strong southerlies bring clean air from the oceans to southern China during the East Asian summer monsoon (EASM) season

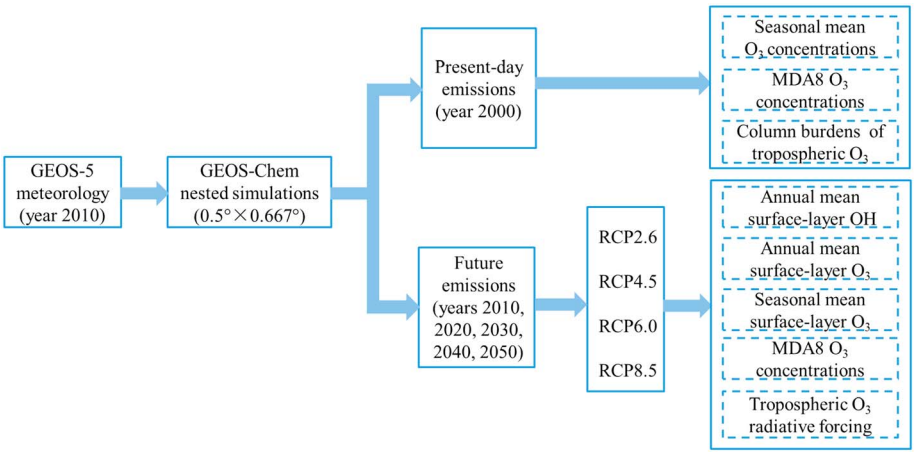

Figure 2. Schematic overview of numerical experiments.

[*He et al.*, 2008; *Wang et al.*, 2011]. It should be noted that simulated O_3 exhibits maximum concentrations of exceeding 70 ppbv in March-April-May (MAM) over the Tibetan Plateau, which can be attributed to the downward transport of O_3 from the stratosphere [*Wild and Akimoto*, 2001]. Simulated high O_3 concentrations in JJA over western China are due to both the large transboundary transport by westerlies and the downward transport from the stratosphere [*Yang et al.*, 2014].

Previous studies [*Wang et al.*, 2011, 2013; *Lou et al.*, 2014; *Yang et al.*, 2014] have shown that the GEOS-Chem model successfully reproduces the spatiotemporal distributions of observed O_3 over China. We conduct comparisons with measurements here to see whether the nested grid version of the GEOS-Chem model with the RCP emissions can capture the magnitudes and spatiotemporal patterns of the observed surface layer O_3.

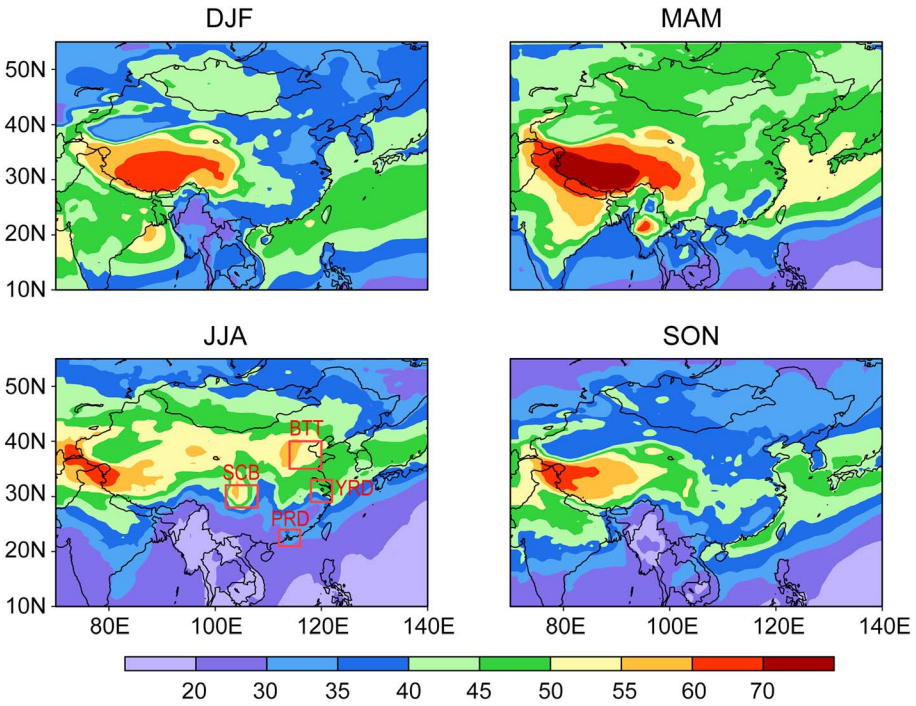

Figure 3. Simulated present-day (year 2000) seasonal mean surface layer O_3 concentrations (ppbv). Also shown in JJA are the four polluted regions examined in this study, including Beijing-Tianjin-Tanggu (BTT, 35°–40°N, 114°–120°E), Yangtze River Delta (YRD, 29°–33°N, 118°–122°E), Pearl River Delta (PRD, 21°–24°N, 112°–116°E), and Sichuan Basin (SCB, 28°–32°N, 102°–108°E).

Table 2. Information for the 10 Chinese Sites With Measurements of Surface Layer O_3 Concentrations Used in Model Evaluation[a]

Station	Location	Observation Period	Reference	MB_2000[b] (ppbv)	NMB_2000[c] (%)	MB_2010 (ppbv)	NMB_2010 (%)
MiYun	40.5°N, 116.8°E	Jan 2006 to Dec 2006	*Wang et al.* [2011]	−1.4	−3.3	−0.5	−1.1
QingDao	36.1°N, 120.3°E	Mar 2004 to Feb 2005	*Yang and Gao* [2008]	+5.2	+13.2	+6.0	+15.2
NanJing	32.2°N, 118.7°E	Jan 2008 to Dec 2008	*Gao et al.* [2012]	+9.9	+29.9	+11.2	+33.9
LinAn	30.4°N, 119.7°E	Aug 1999 to Jul 2000	*Wang et al.* [2011]	+0.4	+0.9	+1.8	+4.4
HokTsui	22.2°N, 114.3°E	Jan 1994 to Dec 2007	*Wang et al.* [2011]	+8.1	+23.1	+10.8	+30.8
JinYunShan	29.8°N, 106.4°E	Jan 2010 to Dec 2010	*Duan et al.* [2011]	+10.9	+31.5	+13.5	+39.2
WaLiGuan	36.3°N, 100.9°E	Aug 1994 to Jul 1995	*Yan et al.* [1997]	+1.2	+2.3	+2.5	+5.1
Shangri-la	28.0°N, 99.4°E	Dec 2007 to Nov 2009	*Ma* [2011]	+0.5	+1.2	+2.4	+5.9
AKeDaLa	47.1°N, 87.9°E	Aug 2004 to Sep 2005	*Lin et al.* [2010]	+6.3	+18.7	+6.6	+19.6
LongFengShan	44.7°N, 127.6°E	Jan 2006 to Dec 2006	*An et al.* [2013]	+3.9	+11.2	+4.5	+12.9

[a]Mean bias (MB, ppbv) and normalized mean bias (NMB, %) between the observations and simulations for year 2000 and year 2010 (under RCP4.5 scenario) are also shown.

[b]$\mathrm{MB} = \left[\sum_{i=1}^{N}(P_i - O_i)\right]/N$, where P_i and O_i are the predicted and observed O_3 concentrations, respectively, i refers to the ith month, and N is the total number of months (i.e., 12).

[c]$\mathrm{NMB} = \left[\sum_{i=1}^{N}(P_i - O_i)\right] / \left(\sum_{i=1}^{N} O_i\right) \cdot 100\%$, where P_i and O_i are the predicted and observed O_3 concentrations, respectively, i refers to the ith month, and N is the total number of months (i.e., 12).

Simulated present-day surface layer O_3 concentrations are compared with year-round measurements at 10 sites in China collected from the literature (Table 2 and Figure 4). Because the measurements at most sites were carried out over years 2000–2010 (Table 2), we show in Figure 4 the simulated concentrations for both year 2000 and year 2010 (under RCP4.5, a medium emission scenario for year 2010). The model successfully reproduces the general features of O_3 seasonality at all sites (Figures 4b–4k). The mean biases (MBs) for year 2000 (2010) are in the range of −1.4 ppbv to +10.9 ppbv (−0.5 ppbv to +13.5 ppbv), and the normalized mean biases (NMBs) are in the range of −3.3% to +31.5% (−1.1% to +39.2%) (Table 2). The scatterplot of simulated year 2000 monthly mean O_3 concentrations versus observations at all the 10 sites is shown in Figure 4l. The model overestimates O_3 concentrations with a MB of +4.5 ppbv and a NMB of +11.6%. The high correlation coefficient of 0.76 indicates that the model captures well the spatiotemporal distributions of observed surface layer O_3 concentrations in China. The MB, NMB, and correlation coefficient between simulations for year 2010 and observations are calculated to be +5.9 ppbv, +15.3%, and 0.75, respectively (the scatterplot for year 2010 is not shown).

3.2. Maximum Daily 8 h Average (MDA8) O_3 Concentrations

We also examine the MDA8 O_3 concentrations, which are often associated with the adverse health effects in epidemiologic studies [*Fann et al.*, 2012; *Yang et al.*, 2012]. Because of the lack of year-round hourly O_3 measurements in China, we evaluate the simulated MDA8 concentrations at three Japanese sites (two remote sites of Ogasawara site (27.1°N, 142.2°E) and Hedo site (26.9°N, 128.2°E) and one urban site of Banryu (34.7°N, 131.8°E)). The measurements are taken from the Acid Deposition Monitoring Network in East Asia (EANET, http://www.eanet.asia/). Figure 5 shows the time series of simulated (for both year 2000 and year 2010 under RCP4.5 scenario) and observed (for year 2010) MDA8 concentrations at these three Japanese sites. The MBs for year 2000 (2010) are in the range of −0.6 ppbv to +2.6 ppbv (0.0 ppbv to +3.1 ppbv), and the NMBs are in the range of −1.6% to +6.3% (0.0% to +7.4%). The model captures well the peaks and troughs of the observed MDA8 concentrations at all three sites, with high correlation coefficients of 0.74–0.87 (for year 2000) and 0.79–0.89 (for year 2010).

3.3. Column Burdens of Tropospheric O_3

Estimates of the radiative effect of O_3 rely on not only ground level concentrations but also tropospheric column burdens. Few ozonesonde observations are available in China [*Chan et al.*, 2003; *Ding et al.*, 2008]. Satellite retrieval has excellent spatial coverage and therefore provides a valuable data set to analyze the spatial distributions of tropospheric O_3. Previous studies have compared tropospheric O_3 simulated by the GEOS-Chem with those retrieved from Tropospheric Emission Spectrometer (TES) [*Zhang et al.*, 2010; *Wang et al.*, 2011], Ozone Monitoring Instrument (OMI) [*Zhang et al.*, 2010], and Global Ozone Monitoring

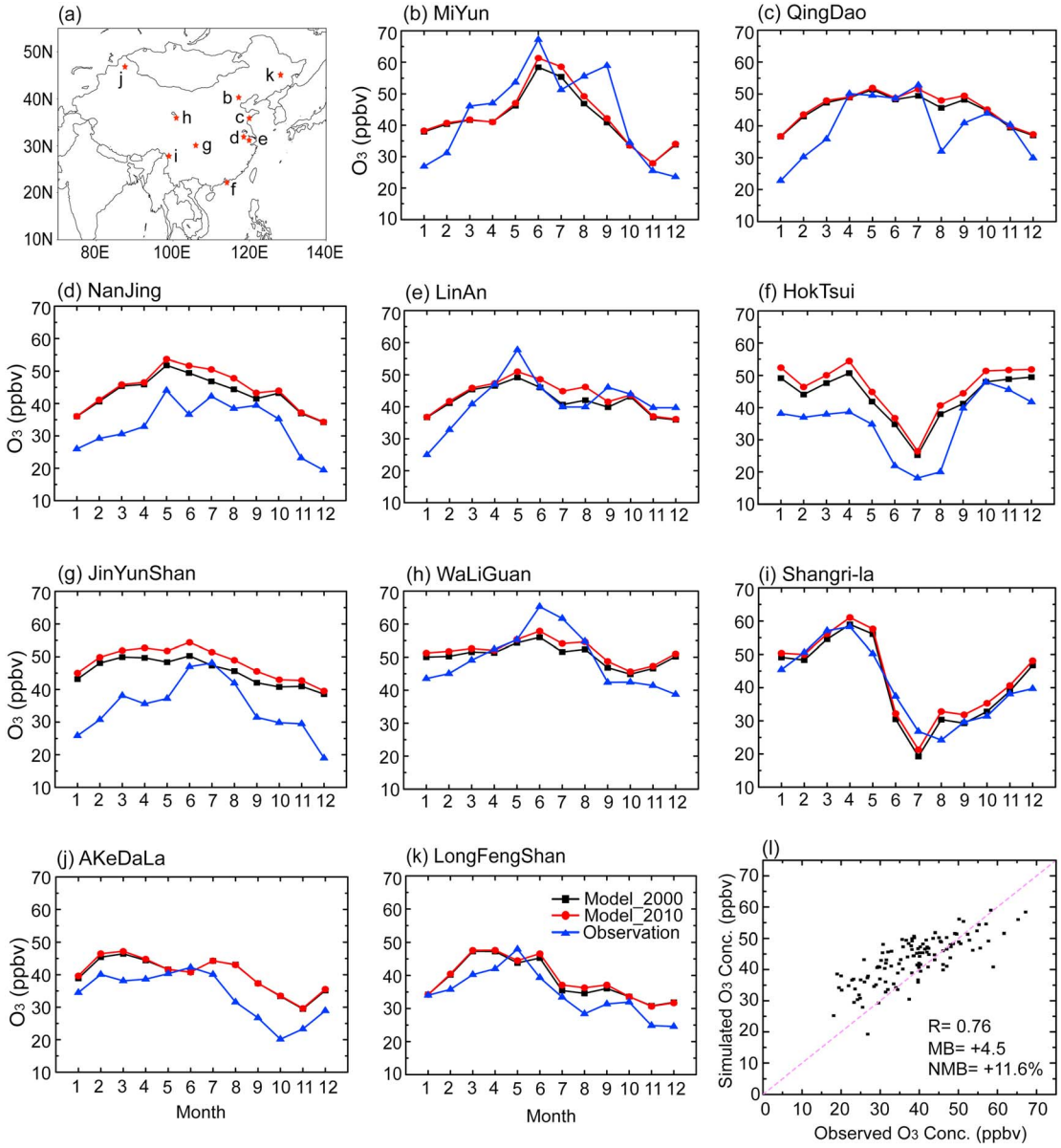

Figure 4. (a) Locations of sites with monthly mean measurements of surface layer O_3 concentrations used for model evaluation. (b–k) Comparisons of simulated year 2000 (black lines) and year 2010 (under RCP4.5 scenario, red lines) surface layer O_3 concentrations (ppbv) with measurements (blue lines) at the sites. (l) The scatterplot of simulated (for year 2000) versus observed monthly mean O_3 concentrations at 10 sites (Figures 4b–4k) over China. Also shown in Figure 4l are the 1:1 line (dashed), mean bias (MB, ppbv), normalized mean bias (NMB), and the correlation coefficient between simulated and observed concentrations (*R*).

Experiment (GOME) [*Liu et al.*, 2006]. All these results show that the GEOS-Chem model captures well the seasonal cycles and spatial distributions of tropospheric O_3 in most regions but has large positive biases in the northern subtropical regions. Here we use tropospheric column ozone (TCO) products retrieved from TES, aboard the EOS Aura satellite launched in July 2004, to evaluate the model performance for tropospheric O_3.

Figure 6 shows maps of annual mean TCO retrieved from TES during 2006−2008 and those simulated by the GEOS-Chem model for year 2000 and year 2010 under RCP4.5 scenario. TES retrievals exhibit high values of 40–55 Dobson units (DU) over central and eastern China and low values of 25–35 DU over the Tibetan Plateau. The spatial distribution of TCO is captured by the model. The simulated high values over the Sichuan Basin were not seen by TES, but other satellite retrievals, such as Total Ozone Mapping Spectrometer/solar backscatter ultraviolet (TOMS/SBUV), had high values at this location [*Wei and Zheng*, 2006; *Li et al.*, 2007]. The differences between the GEOS-Chem simulation and TES observation indicate that

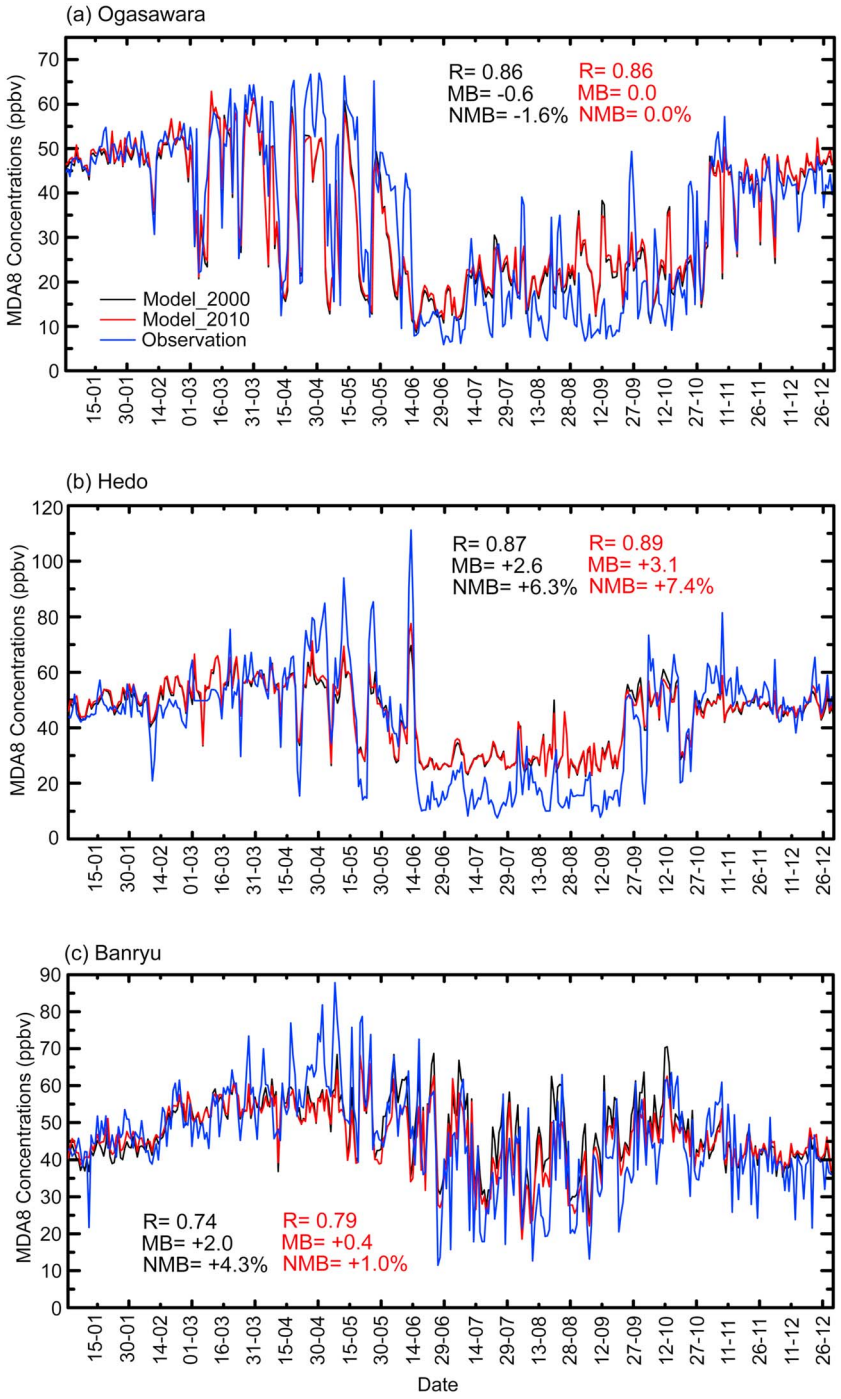

Figure 5. Time series of simulated and observed present-day maximum daily 8 h average (MDA8) O_3 concentrations at three Japanese sites: (a) Ogasawara (27.1°N, 142.2°E), (b) Hedo (26.9°N, 128.2°E), and (c) Banryu (34.7°N, 131.8°E). The model results for year 2000 and year 2010 (under RCP4.5 scenario) are shown by black and red lines, respectively, and observations for year 2010 are shown by blue lines. Correlation coefficient (*R*), mean bias (MB, ppbv), and normalized mean bias (NMB) between simulated and observed MDA8 O_3 concentrations for each station are also shown in each panel (numbers based on year 2000 simulation are in black, and those based on year 2010 simulation are in red).

the model underestimates TCO over the northeastern China by 4–12 DU in simulations for both 2000 and 2010 and overestimates TCO near 30°N by 4–12 DU with year 2000 emissions and by 4–14 DU with year 2010 emissions. *Zhang et al.* [2010] attributed the overestimation of TCO in the northern subtropics in the GEOS-Chem model to excessive stratospheric influx of O_3.

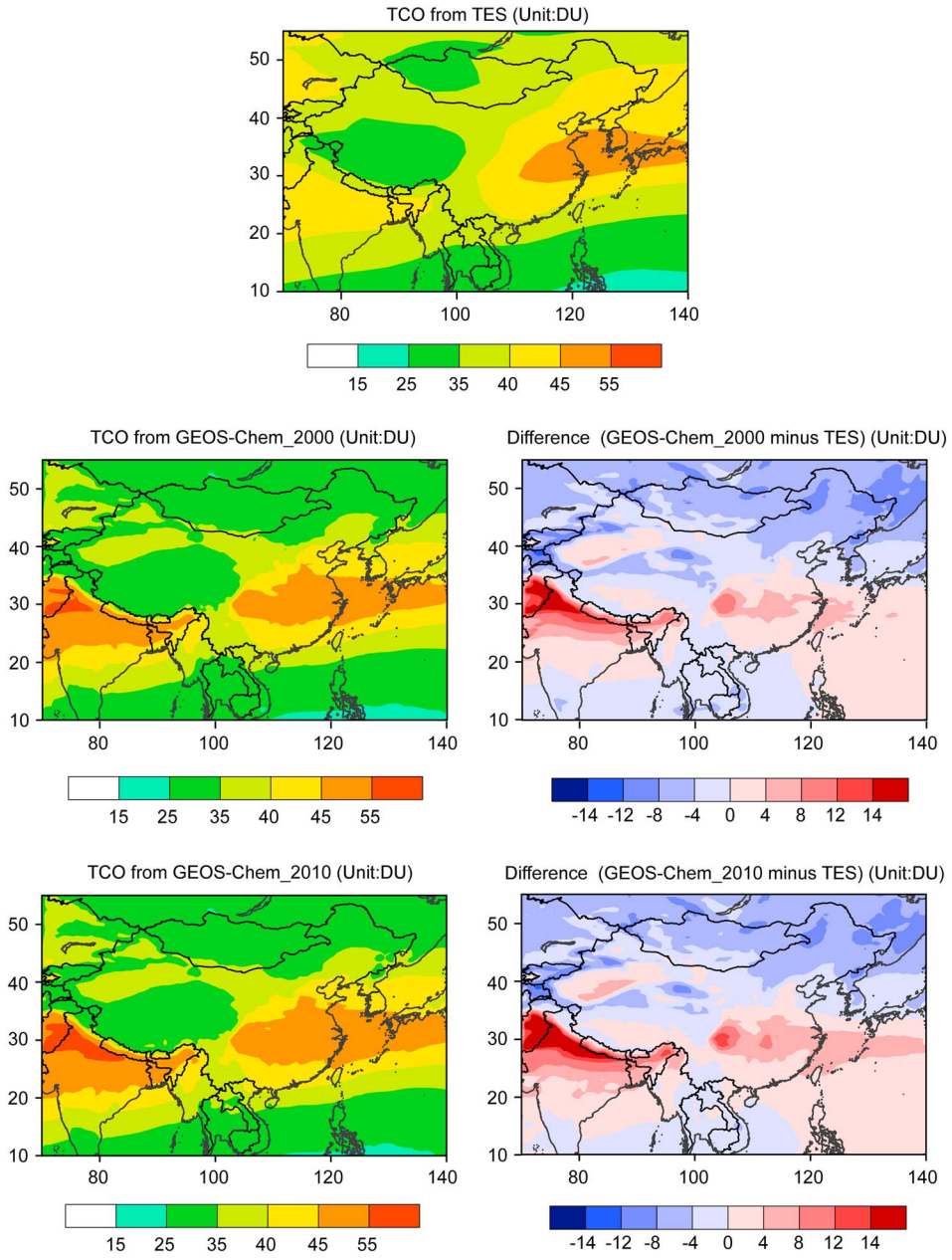

Figure 6. Comparisons of annual mean tropospheric column ozone (TCO, unit: DU) simulated by the GEOS-Chem model with those retrieved from TES. The model results are for year 2000 and year 2010 (under RCP4.5 scenario), and the TES retrievals are the averages over 3 years (2006–2008).

4. Projected Changes in Surface Layer OH Concentrations Over China Under the RCPs

Before looking at future changes in O_3, future changes in hydroxyl radical (OH) over China are examined. As the most active oxidant, OH plays an important role in tropospheric chemistry. The photolysis of O_3 followed by the reaction of excited oxygen atom (O^1D) with water vapor is the most important source of tropospheric OH, and the reaction of $NO+HO_2$ is the second largest source of OH, whereas the reactions of CO and CH_4 with OH comprise the main loss of OH. Therefore, higher emissions of NO_x result in the increases in OH concentrations, but higher emissions of CO and CH_4 tend to lower OH abundance [*Su et al.*, 2012].

Figure 7 shows the projected percentage changes in annual mean surface layer OH concentrations over 2010–2050 for every decade relative to present-day (year 2000) values under the four RCPs.

We emphatically describe here the responses of OH concentrations to changes in emissions in the near future (2030) and future (2050) under the four RCPs. Under RCP2.6, the projected increases in NO_x emissions, decreases in CO emissions, and the lower CH_4 levels all contribute to the overall increases in surface OH over China in 2030. By 2050, OH concentrations are simulated to decrease slightly in southern China due to the dominant role of NO_x reductions but increase slightly in northern China due to the dominant role of CO and CH_4 reductions. As shown in Figure 1d, small changes in CH_4 are projected for 2030 and 2050 under RCP4.5 and RCP6.0. As a result, future changes in NO_x and CO emissions determine OH concentrations under these two scenarios. For RCP4.5, minor changes (within ±12%) in surface OH levels are simulated in 2030, but widespread reductions over China are found in 2050 due to the dominant role of NO_x reductions. The maximum decreases of exceeding 24% are simulated over southeastern China in 2050. Note that the patterns of changes in OH concentrations are quite different for RCP2.6 and RCP4.5, although these two RCPs have very close NO_x and CO emissions in 2050, which can be attributed to the large decreases in CH_4 levels in RCP2.6. Under RCP6.0, increases in NO_x emissions lead to increases in OH concentrations over a large fraction of China in 2030 and 2050, with the largest increases of exceeding 48% in southeastern China and southwestern China by 2050. Significant increases of exceeding 60% in surface OH are simulated over southeastern China in 2030 under the RCP8.5 scenario, which results from the large increases in NO_x emissions from 2000 to 2030. However, high CH_4 levels lead to the reduced OH concentrations over western China in both 2030 and 2050 under RCP8.5. In 2050, the RCP8.5 shows a mixture of positive and negative changes over central and eastern China, which is consistent with the patterns of changes in NO_x emissions (see Figure S1 in the supporting information). The distributions of our simulated changes in surface layer OH concentrations over China in 2050 under RCP2.6 and RCP8.5 are similar to those presented by *Voulgarakis et al*. [2013], but the magnitudes of changes in their study were larger because they presented the changes over 2000–2100.

5. Projected Future O_3 Air Quality Over China Under the RCPs

5.1. Future Changes in Annual Mean Concentrations

Projected changes in annual mean surface layer O_3 concentrations over 2010–2050 for every decade relative to present-day (year 2000) values under the four RCPs are presented in Figure 8. Under RCP2.6, simulated O_3 concentrations increase throughout China in 2010, with the maximum increases of 3–6 ppbv in southern China, but then start to decrease. Reductions in surface layer O_3 concentrations are simulated over almost all of China in years 2030, 2040, and 2050. Significant decreases of exceeding 6 ppbv are simulated over the North China Plain and Sichuan Basin by 2050 due to the reductions in NO_x, CO, NMVOC emissions, and global CH_4 levels.

Under RCP4.5, annual mean surface O_3 concentrations exhibit increases over a large fraction of China in years 2010, 2020, and 2030, with the maximum increases of 3–6 ppbv over southern China in 2020. Concentrations of O_3 are projected to decrease in 2040 and 2050, with maximum decreases of exceeding 6 ppbv over Hunan, Jiangxi provinces, and the Sichuan Basin in 2050. In 2050, the RCP4.5 leads to smaller decreases in surface layer O_3 than the RCP2.6 does, owing to the larger decreases in global CH_4 levels in RCP2.6 since emissions of NO_x, CO, and NMVOCs are approximately the same for RCP2.6 and RCP4.5 (see Figures 1 and S1–S3 in the supporting information).

For RCP6.0, the annual mean surface layer O_3 concentrations increase over 2000–2040 over central, eastern, and southern China and then stabilize over 2040–2050. Significant increases of 6–12 ppbv are simulated over southern China in 2040 and 2050, which can be explained by the considerable increases in emissions of NO_x, CO, and NMVOCs in 2040 and 2050 relative to the present-day values. However, the annual mean O_3 concentrations over western and northern China are projected to decrease slightly (by up to 2 ppbv) in all years except for 2040. These slight decreases in O_3 result from the decreases in transboundary transport from central Asia and Europe. The global modeling study by *Szopa et al*. [2013] projected decreases in surface O_3 over the Northern Hemisphere except for China and Indonesia under RCP6.0.

The RCP8.5 leads to overall increases in annual mean O_3 concentrations over China in all the future years simulated. Concentrations of O_3 reach peak values in 2020 and 2030, with the maximum increases of 6–12 ppbv in southern China as a result of the considerable increases in NO_x, CO, NMVOCs emissions, and

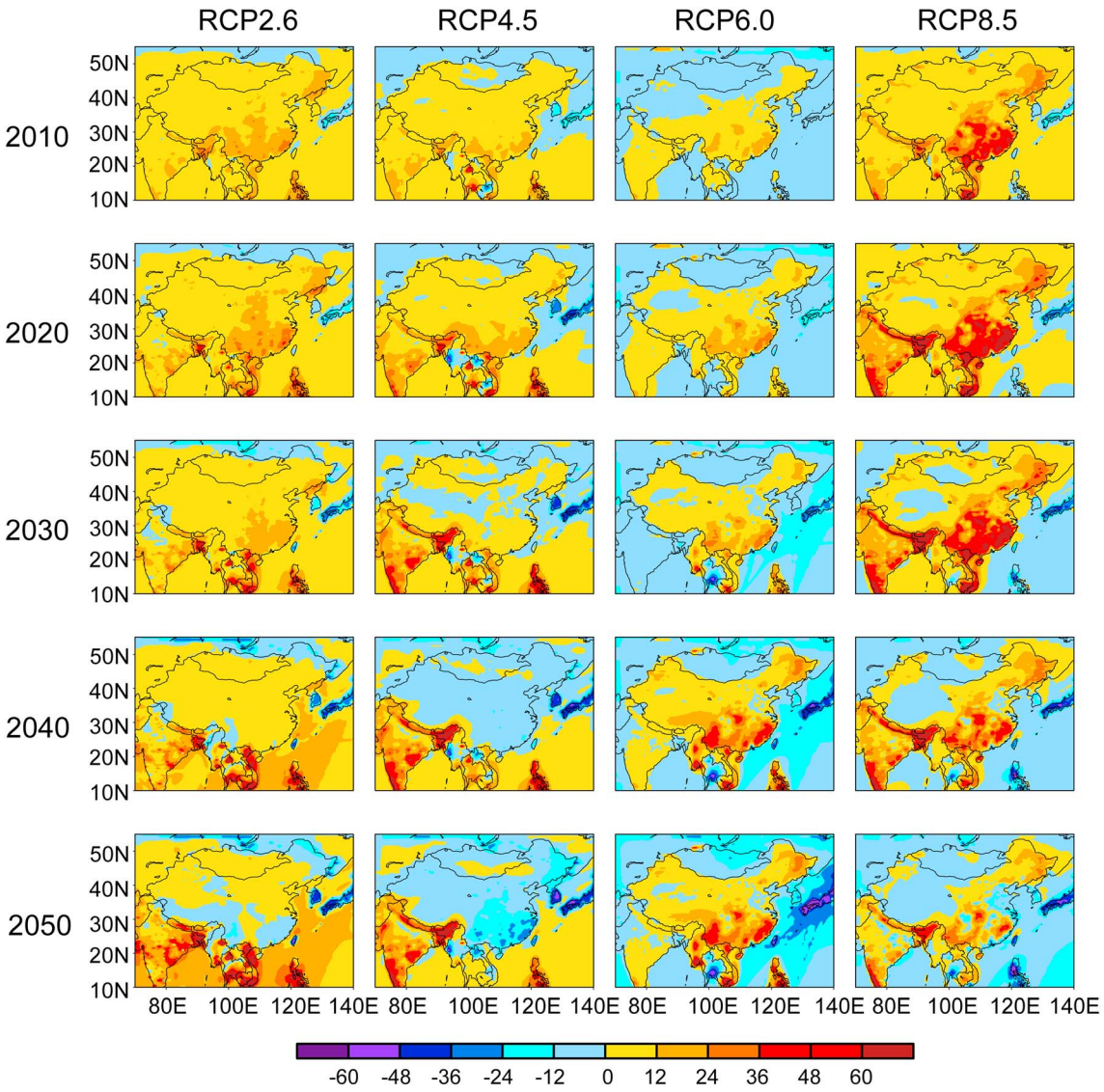

Figure 7. Percentage changes in annual mean surface layer OH concentrations (%) over 2010–2050 for every decade relative to present-day (year 2000) values under the four RCPs.

global CH_4 levels from 2000 to 2020 (and 2030). In spite of extremely high CH_4 levels, year 2050 O_3 concentrations show small increases of 0–3 ppbv over eastern China owing to the significant decreases in emissions of NO_x, CO, and NMVOCs after 2030 (Figure 1).

The projected maximum changes in annual mean surface layer O_3 concentrations in China over 2000–2030 in our study are, respectively, −4, +6, and +12 ppbv under RCP2.6, RCP4.5, and RCP8.5, which agree with the multimodel mean maximum changes −5, +7, and +10 ppbv over the same years under these scenarios presented by *Young et al.* [2013b]. Under RCP6.0, multimodel mean O_3 concentrations exhibit statistically nonsignificant changes over southern China in *Young et al.* [2013b], while a maximum increase of 6 ppbv is simulated in southern China in our work. For 2050 under RCP6.0, *Szopa et al.* [2013] presented a maximum increase in O_3 of 6 ppbv, while our model simulates a maximum increase of 12 ppbv. The larger increases in O_3 in our study can be attributed in part to the higher horizontal resolution of our model.

5.2. Future Changes in Seasonal Mean Concentrations Over the Four Heavily Polluted Regions

Figure 9 shows evolutions of changes in seasonal mean surface O_3 levels over 2010–2050 relative to 2000 averaged over the four heavily polluted regions, including BTT, YRD, PRD, and SCB. The domains of these four

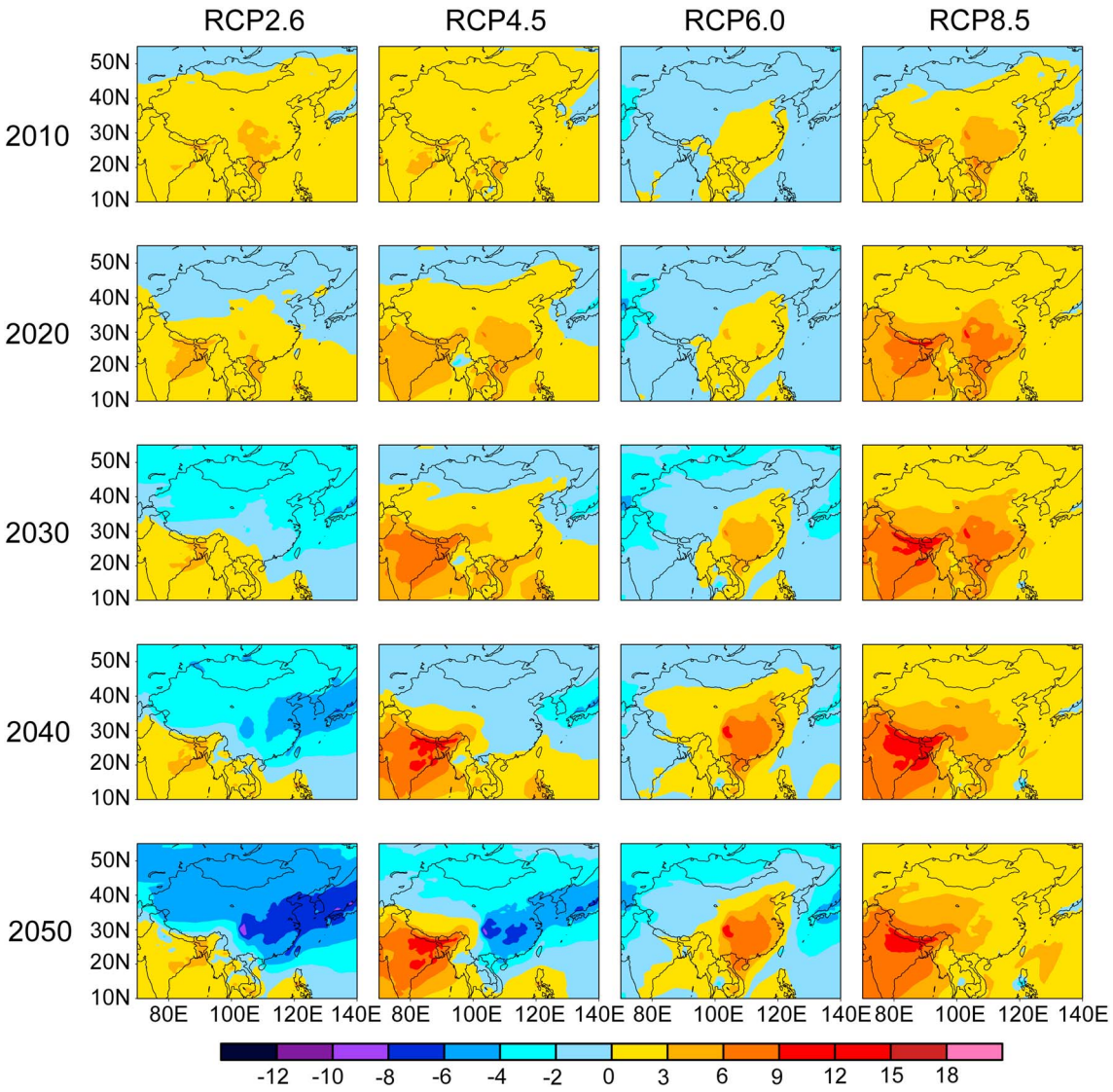

Figure 8. Predicted changes in annual mean surface layer O_3 concentrations (ppbv) over 2010–2050 for every decade relative to present-day (year 2000) values under the four RCPs.

regions are marked in Figure 3. Figure 10 shows the maximum percentage changes in seasonal mean O_3 concentrations and the years in which these maximum percentage changes occur, as the changes in the four heavily polluted regions are calculated relative to the present-day (year 2000) values. Over BTT, the surface layer O_3 concentrations exhibit the largest changes in JJA among all the seasons because of the most active photochemical reactions in this season. The patterns of future changes in O_3 concentrations in JJA mimic those of future changes in annual emissions of NO_x, CO, and NMVOCs (Figure 1). The largest changes in JJA surface layer O_3 over BTT are simulated to be −8.7 ppbv (−16.5%) in 2050, −8.3 ppbv (−15.7%) in 2050, +12.2 ppbv (+23.2%) in 2050, and +10.3 ppbv (+19.5%) in 2030 under RCP2.6, RCP4.5, RCP6.0, and RCP8.5 (Figures 9 and 10), respectively. Compared with JJA O_3, the future changes in O_3 in other three seasons over BTT are much smaller. From 2000 to 2010, simulated DJF O_3 concentrations in BTT are projected to decrease slightly under RCP2.6, RCP6.0, and RCP8.5. In DJF, biogenic VOC emissions are especially low over BTT, whereas anthropogenic NO_x emissions are fairly high due to the residential heating, leading to low VOCs/NO_x ratio in this region [*Lou et al.*, 2010]. Therefore, the projected increases in NO_x emissions lead to decreases in O_3 concentrations in DJF. Over 2000–2050, changes in O_3 concentration in BTT are in the ranges of −4.0 to +2.2 ppbv in DJF, −6.8 to +1.8 ppbv in MAM, and −5.8 to +2.9 ppbv in September-October-November (SON).

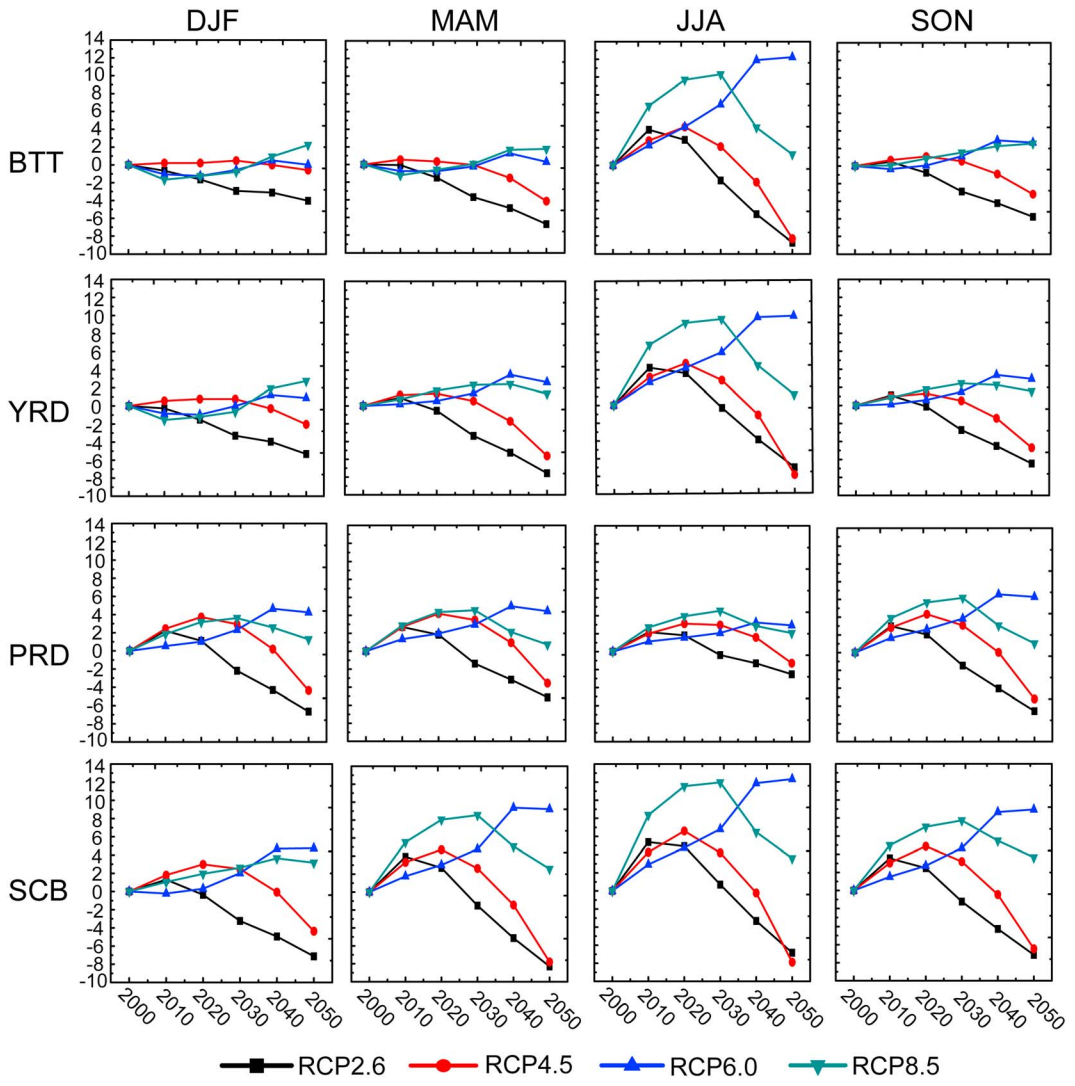

Figure 9. Future changes in seasonal mean surface O_3 levels (ppbv) over 2010–2050 relative to 2000 over the polluted regions of BTT, YRD, PRD, and SCB under the four RCPs.

Over YRD, the trends and magnitudes of future changes in surface layer O_3 are quite close to those over BTT. The surface O_3 over YRD also exhibits the largest changes in JJA; the largest changes are simulated to be −7.1 ppbv (−16.4%) in 2050, −7.9 ppbv (−18.3%) in 2050, +10.0 ppbv (+23.0%) in 2050, and +9.6 ppbv (+22.3%) in 2030 under RCP2.6, RCP4.5, RCP6.0, and RCP8.5, respectively. In DJF, MAM, and SON, future changes in O_3 over YRD are slightly larger than those over BTT as a result of stronger photochemical reactions over YRD (YRD is located over 29°–33°N, while BTT is over 35°–40°N).

Future changes in O_3 over PRD exhibit similar trends in all seasons, with the largest percentage changes in SON due to the relatively strong photochemical production. Increasing clouds associated with the EASM rainfall suppress photochemical production of O_3 over southern China by altering solar radiation [*Lin et al.*, 2009; *Zhao et al.*, 2010], leading to the smallest future changes in surface O_3 concentrations in JJA over PRD. The largest changes in SON surface layer O_3 over PRD are simulated to be −6.6 ppbv (−15.5%) in 2050, −5.2 ppbv (−12.3%) in 2050, +6.6 ppbv (+15.5%) in 2040, and +6.2 ppbv (+14.6%) in 2030 under RCP2.6, RCP4.5, RCP6.0, and RCP8.5, respectively. Note that over PRD, future changes in O_3 in DJF are just slightly smaller than those in SON because of the low latitudes and hence strong photochemistry in DJF.

Over SCB, the magnitudes of future changes in surface layer O_3 concentrations are large in all seasons, owing to the large future changes in precursor emissions in this region (see Figures S1–S3 in the supporting

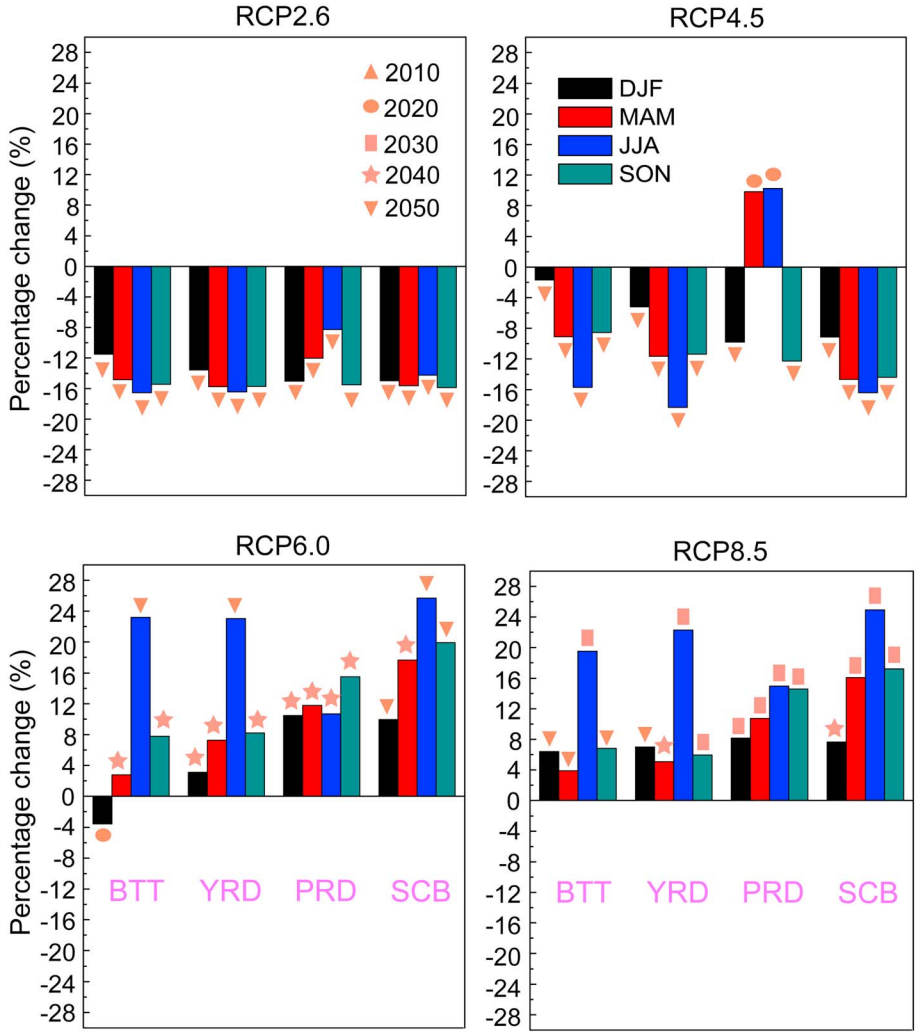

Figure 10. The maximum percentage changes (%) in seasonal mean O_3 concentrations and the years in which these maximum percentage changes occur, as the changes in the four heavily polluted regions are calculated relative to the present-day (year 2000) values. The maximum percentage changes are shown by colored columns, and the years are denoted by orange symbols.

information) and high present-day O_3 levels throughout the year due to the unique terrain of the Sichuan Basin [*Wei and Zheng*, 2006]. The simulated surface layer O_3 concentrations exhibit the largest changes in JJA; the largest changes in JJA O_3 over SCB are simulated to be −6.8 ppbv (−14.2%) in 2050, −7.9 ppbv (−16.4%) in 2050, +12.3 ppbv (+25.7%) in 2050, and +12.0 ppbv (+24.9%) in 2030 under RCP2.6, RCP4.5, RCP6.0, and RCP8.5, respectively.

5.3. Future Changes in MDA8 O_3 Concentrations Over the Four Heavily Polluted Regions

The new Chinese National Ambient Air Quality Standard (NAAQS, GB 3095-2012) has set up an O_3 air quality standard of 160 $\mu g\,m^{-3}$ (i.e., 74.7 ppbv at 273 K and 1013 hPa) for MDA8. The number of MDA8 exceedance days is used as a measure for the potential health impacts of O_3. An exceedance day is defined as a day with the MDA8 O_3 concentration larger than 74.7 ppbv according to the NAAQS.

We show in Figure 11 the numbers of MDA8 exceedance days over 2000–2050 in the four heavily polluted regions under the four RCPs. The numbers of exceedance days for present day (year 2000) are simulated to be 10, 0, 0, and 2 days over BTT, YRD, PRD, and SCB, respectively. The evolutions of numbers of exceedance days mimic those of anthropogenic emissions (NO_x, CO, and NMVOCs). Under RCP2.6 and RCP4.5, no exceedance days are found in 2050 over the four polluted regions, indicating that the reductions in emissions

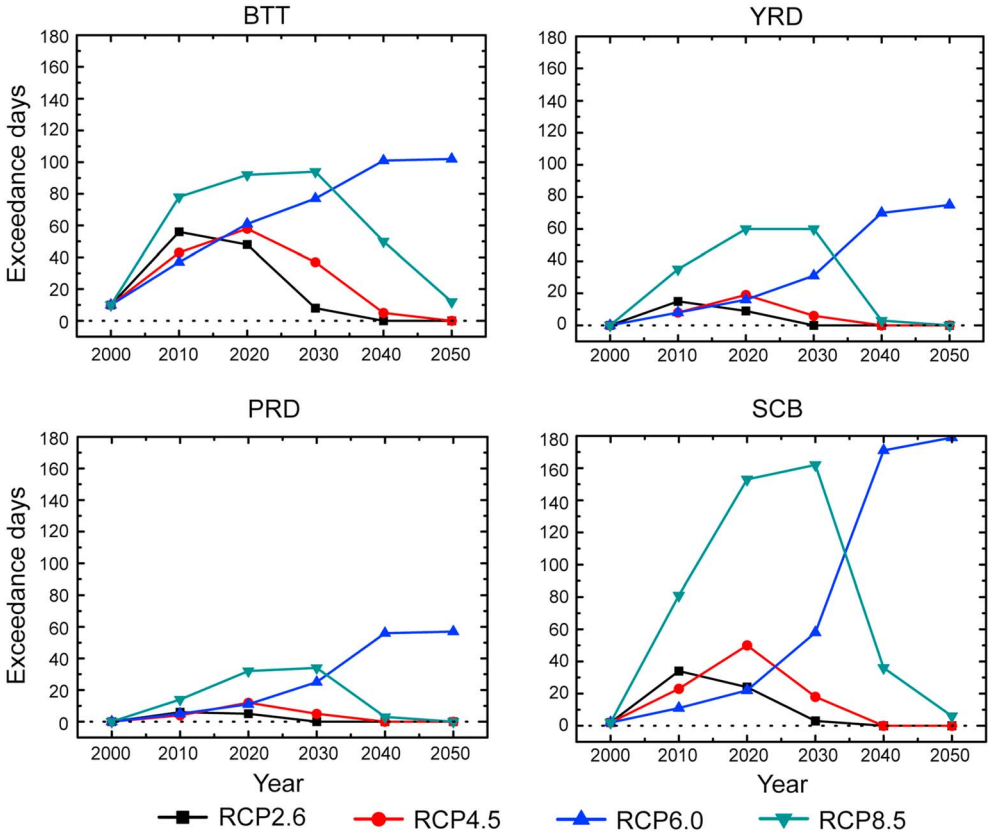

Figure 11. Numbers of O_3 exceedance days (days with the maximum daily 8 h average (MDA8) O_3 concentrations exceeding 74.7 ppbv) over 2000–2050 in the four heavily polluted regions under the four RCPs. The dotted line at the bottom of each panel represents that the number of exceedance day is 0.

of O_3 precursors (NO_x, CO, and NMVOCs) are highly effective in limiting numbers of exceedance days under these two RCP scenarios. The RCP6.0 leads to significant increases in numbers of exceedance days over 2000–2050; the numbers of exceedance days in 2050 over the four polluted regions of BTT, YRD, PRD, and SCB are calculated to be 102, 75, 57, and 179 days, respectively. Note that the future numbers of exceedance days in individual locations within a region (e.g., BTT) could be higher than the average across this region. For RCP8.5, the projected numbers of exceedance days reach the maximum in 2030 and then rapidly decrease due to the substantial reductions in NO_x, CO, and NMVOCs emissions after 2030. The numbers of exceedance days under RCP8.5 in 2030 (2050) are projected to be 94, 60, 34, and 162 (12, 0, 0, and 6) days over BTT, YRD, PRD, and SCB, respectively.

Cumulative probability distributions of simulated MDA8 O_3 concentrations averaged over the four heavily polluted regions for present day (year 2000) and year 2050 under the four RCPs are shown in Figure 12. Compared with present day, the cumulative probability distributions of MDA8 O_3 concentrations under RCP2.6 and RCP4.5 shift to lower values, indicating reduced MDA8 concentrations under the emission reduction scenarios of RCP2.6 and RCP4.5. Under RCP6.0, the MDA8 shows small changes in the low tail of the distribution but large increases in the high tail of the distribution, indicating more peak O_3 episodes owing to the substantial increases in anthropogenic emissions in NO_x, CO, and NMVOCs. Despite the significant increases in global CH_4 levels, few changes are found in 2050 under RCP8.5 due to small changes in the emissions of NO_x, CO, and NMVOCs.

6. Future Changes in Tropospheric O_3 Radiative Forcing Over China

The radiative forcing (RF) is calculated as the change in net radiation flux at the tropopause by anthropogenic emissions. All simulations use the same meteorological fields of year 2010. Figure 13 shows the simulated

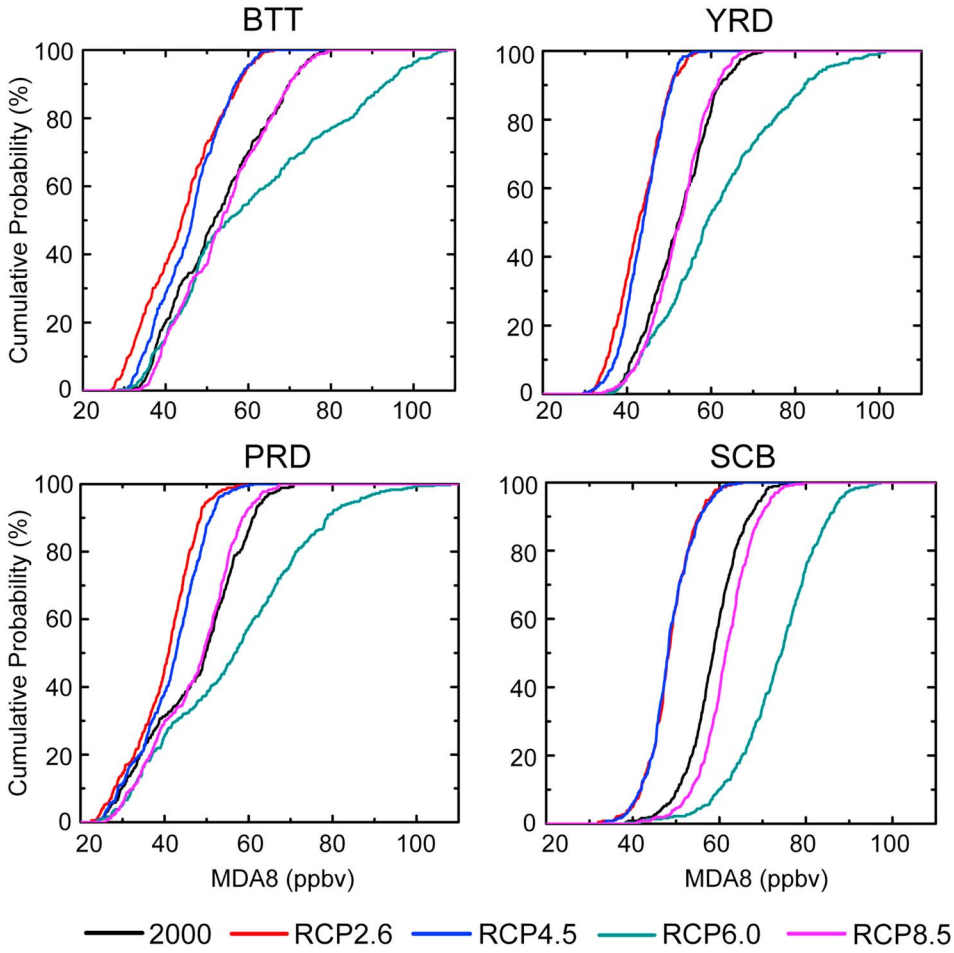

Figure 12. Cumulative probability distributions of simulated maximum daily 8 h average (MDA8) O_3 concentrations averaged over the four heavily polluted regions for present day (year 2000, black line) and year 2050 under the four RCPs (color lines).

present-day annual mean RF by tropospheric O_3 at the tropopause (year 2000 relative to 1850). For preindustrial times, all anthropogenic emissions are shut off and the global mean CH_4 concentration of 0.7 ppm is used in the simulation of O_3. The geographical distribution of simulated present-day RF resembles that of tropospheric column burden of O_3 (Figure 6), with high RF values over the central and eastern China of 0.6–0.8 W m^{-2} and low values over the Tibetan Plateau of 0.2–0.4 W m^{-2}, which agree with those reported by *Wu et al*. [2002], *Stevenson et al*. [2013], and *Szopa et al*. [2013]. The highest RF values of 0.7–0.8 W m^{-2} are simulated over the Sichuan Basin and the Hunan-Hubei-Jiangxi provinces. Table 3 compares our estimated present-day RF values over China with those reported in previous studies. The tropospheric O_3 RF averaged over eastern China (18°–45°N, 95°–125°E) is 0.58 W m^{-2} in this work, close to the value of 0.53 W m^{-2} estimated by *Chang and Liao* [2009], who also used the IPCC AR5 emissions inventory for year 2000. With respect to the maximum RF values over China, our estimated values of 0.7–0.8 W m^{-2} are close to those estimated by *Hauglustaine and Brasseur* [2001] and *Szopa et al*. [2013] but higher than those obtained by other studies listed in Table 3. The differences in the maximum RF values in different studies can be explained in part by the different horizontal resolutions of the models and the discrepancies in anthropogenic emissions.

Projected future changes in annual mean tropospheric O_3 RF at the tropopause over 2010–2050 for every decade relative to 2000 under the four RCPs are presented in Figure 14. The patterns of changes in tropospheric O_3 RF are similar to those of changes in tropospheric column O_3 (see Figure S4 in the supporting information). Relative to present day, projected O_3 RF increases in 2010 and 2020 and decreases over 2030–2050 throughout China under RCP2.6. Large decreases of 0.15–0.2 W m^{-2} are simulated over the

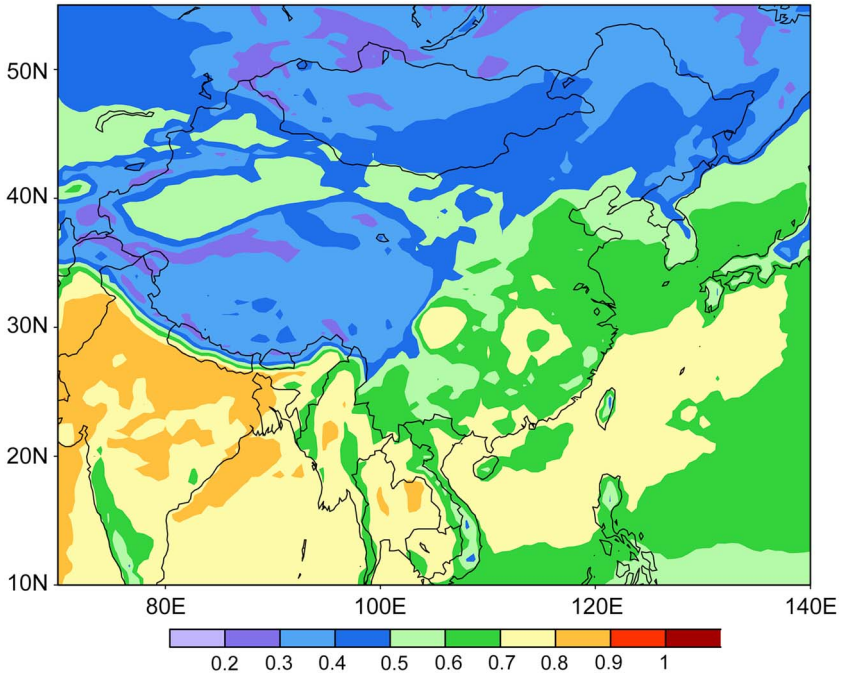

Figure 13. Simulated annual mean tropospheric O_3 radiative forcing (W m^{-2}) at the tropopause for present day (year 2000) relative to preindustrial times (year 1850).

North China Plain by 2050 due to the large reductions in tropospheric column O_3 in this region. Under RCP4.5, annual mean O_3 RF exhibits moderate increases of 0.05–0.15 W m^{-2} over southern China and slight increases of 0–0.05 W m^{-2} over northern China in years 2010, 2020, 2030, and 2040 and small changes in 2050. For RCP6.0, minor decreases of up to 0.05 W m^{-2} are found over a large fraction of China in years 2010, 2020, and 2030, whereas moderate increases of 0.05–0.1 W m^{-2} are simulated over southern China in 2040 and 2050. The RCP8.5 leads to overall increases in O_3 RF throughout China in all the future years, with the maximum increases of 0.2–0.25 W m^{-2} in the Sichuan Basin in years 2030, 2040, and 2050. Under RCP8.5, although small increases in surface layer O_3 concentrations are simulated for 2050, the large

Table 3. Comparisons of the Simulated Annual Mean Tropospheric O_3 Radiative Forcing Over China in This Work With the Values Reported in Previous Studies[a]

				Radiative Forcing (W m^{-2})	
Reference	Model	Year	Region	Annual Mean[b]	Maximum Value[c]
This study	GEOS-Chem	1850–2000	China	0.48	0.7–0.8
			Eastern China (18°–45°N, 95°–125°E)	0.58	
Berntsen et al. [2000]	OsloC TM-1	1850–1990	Southeast Asia	0.45	0.6–0.7
Wang et al. [2005]	RegCM2	1860–2000	China and its adjacent area (6°–52°N, 85°–130°E)	0.65	NA
Chang et al. [2009]	GISS GCM II′	1950–2000	Eastern China (20°–50°N, 100°–130°E)	0.87	
Chang and Liao [2009]	GISS GCM II′	1850–2000	Eastern China (18°–45°N, 95°–125°E)	0.53	
Stevenson et al. [2013]	Multimodel mean	1850–2000	China	NA	0.6–0.7
Hauglustaine and Brasseur [2001]	MOZART	Preindustrial–Present			0.7–0.75
Szopa et al. [2013]	IPSL-CM5 Earth System Model	1850–2000			0.75–0.85
Shindell et al. [2003]	GISS GCM	1850–1990			0.55–0.7
Cionni et al. [2011]	CAM3.5 and GISS-PUCCINI	1850–2000			0.45–0.6

[a]NA: not available.
[b]Annual mean tropospheric O_3 radiative forcing is averaged over the region shown in this table.
[c]Maximum value means the largest annual mean tropospheric O_3 radiative forcing found over the domain of China.

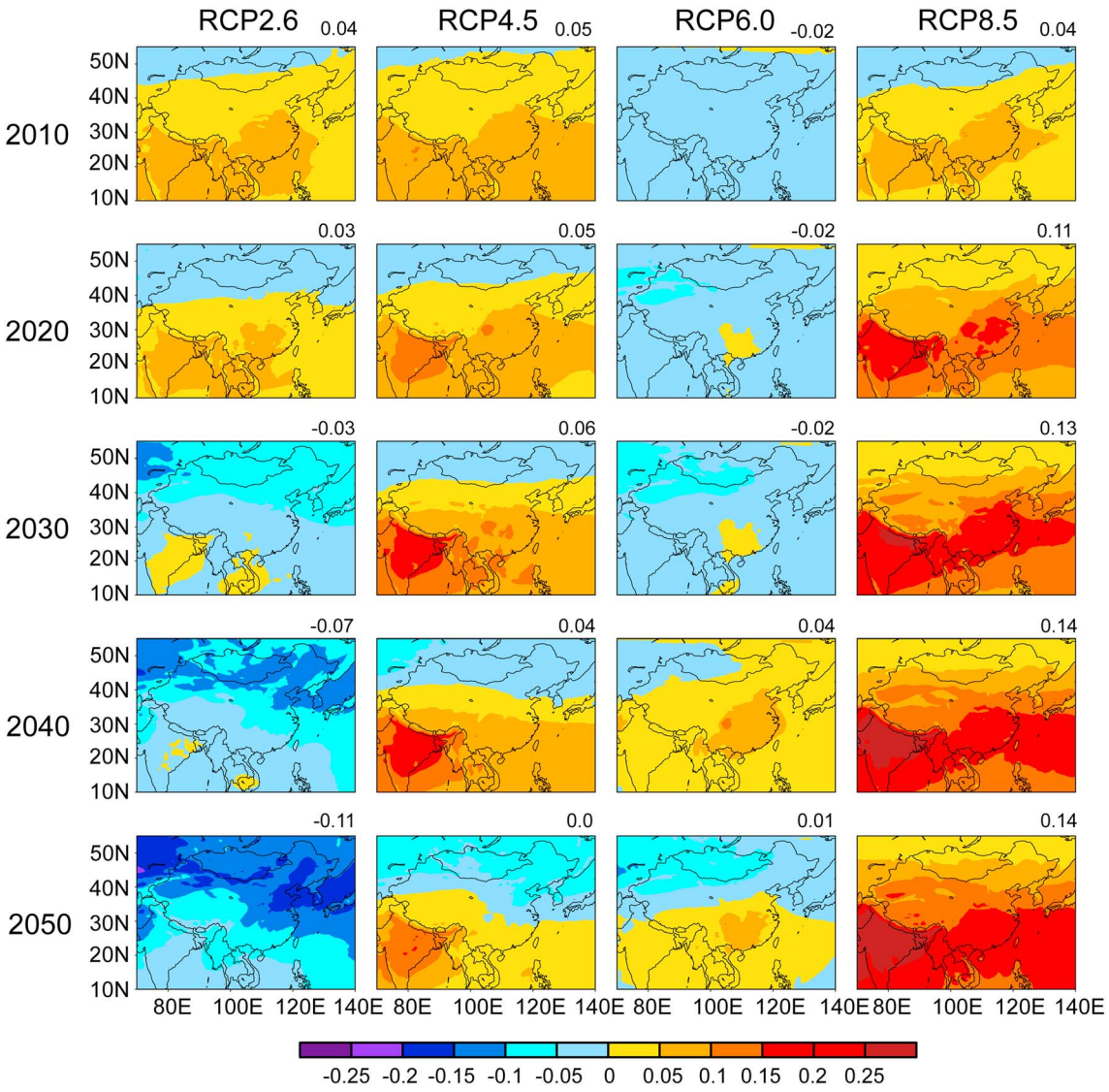

Figure 14. Projected changes in annual mean tropospheric O_3 radiative forcing ($W\,m^{-2}$) at the tropopause over 2010–2050 for every decade (relative to year 2000) under the four RCPs. The annual mean O_3 radiative forcing (relative to year 2000) averaged over eastern China (18°–45°N, 95°–125°E) is shown on the top right corner of each panel.

increases in tropospheric column O_3 lead to high values of tropospheric O_3 RF in this year. The large increases of TCO over China can be attributed to the increases in long-distance transport of tropospheric O_3. Under RCP 8.5, while surface layer O_3 over China peaks at 2030 (Figure 8), the global tropospheric O_3 burden and tropospheric O_3 RF were projected to increase monotonically over 2000–2050 under RCP8.5 by global simulations [*Kawase et al.*, 2011; *Stevenson et al.*, 2013; *Szopa et al.*, 2013; *Young et al.*, 2013a]. Relative to 2000, year 2050 tropospheric O_3 RF averaged over eastern China (18°–45°N, 95°–125°E) is calculated to be -0.11, 0.0, 0.01, and $0.14\,W\,m^{-2}$ for RCP2.6, RCP4.5, RCP6.0, and RCP8.5, respectively. *Hansen et al.* [2007] simulated increases in temperature in eastern China by up to 0.6 K over 1880–2003 as the global mean tropospheric O_3 RF was $0.44\,W\,m^{-2}$, and *Chang et al.* [2009] predicted a warming of 0.43°C over 1950–2000 by a tropospheric O_3 RF of $0.87\,W\,m^{-2}$ when both the forcing and warming were averaged over eastern China. The four RCP scenarios predict a wide range of possible future changes in tropospheric O_3 RF, from $-0.11\,W\,m^{-2}$ under RCP2.6 to $0.14\,W\,m^{-2}$ under RCP 8.5 in 2050 relative to 2000, which provides options for improving O_3 air quality while mitigating warming over eastern China from 2000 to 2050.

7. Conclusions

We use the high-resolution nested grid version of the GEOS-Chem model (0.5° latitude by 0.667° longitude) to simulate 2000–2050 changes in ground level O_3 concentrations, numbers of O_3 exceedance days, and tropospheric O_3 RF over China in response to the changes in anthropogenic emissions under the RCPs (RCP2.6, RCP4.5, RCP6.0, and RCP8.5). Comparisons of the simulated present-day (year 2000) O_3 concentrations with measurements show that the model can capture the spatiotemporal distributions of the observed surface layer O_3 concentrations in China, with a NMB of +11.6% and a high correlation coefficient of 0.76.

Future changes in annual mean surface layer O_3 concentrations are examined first. Over China, RCP8.5 is the worst scenario for near future (2020–2030) and RCP6.0 is the worst scenario over 2040–2050. Future changes in seasonal mean surface layer O_3 concentrations exhibit different trends and magnitudes in the four heavily polluted regions. The trends and magnitudes of future changes in surface O_3 are quite close over BTT and YRD. Over these two regions, the simulated O_3 concentrations show largest future changes in JJA among all the seasons; the largest changes in JJA surface layer O_3 over BTT (YRD) are simulated to be −16.5% (−16.4%) in 2050, −15.7% (−18.3%) in 2050, +23.2% (+23.0%) in 2050, and +19.5% (+22.3%) in 2030 under RCP2.6, RCP4.5, RCP6.0, and RCP8.5, respectively. Future changes in O_3 over PRD have similar trends and magnitudes in DJF, MAM, and SON; future changes in these seasons are large owing to the strong photochemistry throughout the year because of the low latitudes of PRD. Increasing clouds associated with the EASM rainfall suppress photochemical production of O_3 and lead to the smallest future changes in surface O_3 concentrations in JJA over PRD. Over SCB, the magnitudes of future changes in surface layer O_3 concentrations are large in all seasons because of the large future changes in precursor emissions and high present-day O_3 levels throughout the year. The largest changes in JJA O_3 over SCB are simulated to be −14.2% in 2050, −16.4% in 2050, +25.7% in 2050, and +24.9% in 2030 under RCP2.6, RCP4.5, RCP6.0, and RCP8.5, respectively.

We then examine MDA8 O_3 concentrations in the four heavily polluted regions. In present day (year 2000), the numbers of MDA8 O_3 exceedance days are simulated to be 10, 0, 0, and 2 days over BTT, YRD, PRD, and SCB, respectively. The future changes in numbers of exceedance days mimic those in anthropogenic emissions (NO_x, CO, and NMVOCs). In the near future (year 2030), the numbers of exceedance days are the highest under RCP8.5, followed by RCP6.0. The numbers are calculated to be 94, 60, 34, and 162 days under RCP8.5 and 77, 31, 25, and 58 days under RCP6.0 over BTT, YRD, PRD, and SCB, respectively. In year 2050, no or very small numbers of exceedance days are found in the four heavily polluted regions under RCP2.6, RCP4.5, and RCP8.5, but extremely high numbers of exceedance days of 102, 75, 57, and 179 days are simulated over BTT, YRD, PRD, and SCB, respectively, under RCP6.0.

Future changes in annual mean tropospheric O_3 RF at the tropopause are also examined. Averaged over eastern China (18°–45°N, 95°–125°E), year 2000 radiative forcing relative to year 1850 is calculated to be 0.58 W m^{-2}. The patterns of future changes in tropospheric O_3 RF resemble those of changes in tropospheric column O_3. Relative to 2000, year 2050 tropospheric O_3 RF averaged over eastern China under the RCP2.6, RCP4.5, RCP6.0, and RCP8.5 is calculated to be −0.11, 0.0, 0.01, and 0.14 W m^{-2}, respectively.

When we consider both the health and climate impacts of tropospheric O_3 in 2050 over China, RCP2.6 is a significantly improving scenario for both air quality and climate, with zero MDA8 O_3 exceedance days over the four heavily polluted regions and a tropospheric O_3 RF of −0.11 W m^{-2} over eastern China (relative to 2000). RCP4.5 is a significantly improving scenario for air quality but has small impact on climate, with zero exceedance days and a regional mean tropospheric O_3 RF of 0.0 W m^{-2}. RCP6.0 is a significantly worsening scenario for air quality and a slightly worsening scenario for climate, with 179 exceedance days over the SCB and a regional tropospheric O_3 RF of 0.01 W m^{-2}. RCP8.5 is a slightly worsening scenario for air quality and a significantly worsening scenario for climate, with 12 exceedance days over BTT and a tropospheric O_3 RF of 0.14 W m^{-2} over eastern China. Therefore, to simultaneously abate air pollution and climate warming induced by O_3, both the anthropogenic emissions of NO_x, CO, NMVOCs, and global CH_4 levels should be reduced, as represented by RCP2.6.

In this study we are focused on how tropospheric O_3 over China responds to future changes in anthropogenic emissions alone by using the same year 2010 meteorology in all the simulations. It should be noted that future O_3 levels are also influenced by future interannual to decadal timescale climate change

[*Liao et al.*, 2006; *Kurokawa et al.*, 2009], especially for the high O_3 episodes [*Racherla and Adams*, 2009]. Future climate change can also influence tropospheric O_3 by altering the stratospheric influx [*Sudo et al.*, 2003; *Young et al.*, 2013a]. These are the uncertainties in our results that need to be addressed in future studies.

Acknowledgments

This work was supported by the National Basic Research Program of China (973 program, grant 2014CB441202), the Strategic Priority Research Program of the Chinese Academy of Sciences (grant XDA05100503), and the National Natural Science Foundation of China under grants 91544219, 41475137, and 41321064. Observations at Japanese sites were provided by the Acid Deposition Monitoring Network in East Asia (EANET, http://www.eanet.asia/), and the TES data were obtained from the NASA Langley Research Center Atmospheric Science Data Center (https://eosweb.larc.nasa.gov/). We are very grateful to the reviewers for their helpful comments and thoughtful suggestions.

References

Alexander, B., R. J. Park, D. J. Jacob, Q. B. Li, R. M. Yantosca, J. Savarino, C. C. W. Lee, and M. H. Thiemens (2005), Sulfate formation in sea-salt aerosols: Constraints from oxygen isotopes, *J. Geophys. Res.*, *110*(D10), D10307, doi:10.1029/2004JD005659.

An, X., Z. Sun, W. Lin, M. Jin, and N. Li (2013), Emission inventory evaluation using observations of regional atmospheric background stations of China, *J. Environ. Sci.*, *25*(3), 537–546, doi:10.1016/S1001-0742(12)60082-5.

Berntsen, T. K., G. Myhre, F. Stordal, and I. S. A. Isaksen (2000), Time evolution of tropospheric ozone and its radiative forcing, *J. Geophys. Res.*, *105*(D7), 8915–8930, doi:10.1029/1999JD901139.

Bey, I., D. J. Jacob, R. M. Yantosca, J. A. Logan, B. Field, A. M. Fiore, Q. Li, H. Liu, L. J. Mickley, and M. Schultz (2001), Global modeling of tropospheric chemistry with assimilated meteorology: Model description and evaluation, *J. Geophys. Res.*, *106*(D19), 23,073–23,095, doi:10.1029/2001JD000807.

Brasseur, G. P., M. Schultz, C. Granier, M. Saunois, T. Diehl, M. Botzet, E. Roeckner, and S. Walters (2006), Impact of climate change on the future chemical composition of the global troposphere, *J. Clim.*, *19*(16), 3932–3951, doi:10.1175/JCLI3832.1.

Butler, T. M., Z. S. Stock, M. R. Russo, H. A. C. Denier van der Gon, and M. G. Lawrence (2012), Megacity ozone air quality under four alternative future scenarios, *Atmos. Chem. Phys.*, *12*, 4413–4428, doi:10.5194/acp-12-4413-2012.

Chan, C. Y., L. Y. Chan, W. L. Chang, Y. G. Zheng, H. Cui, X. D. Zheng, Y. Qin, and Y. S. Li (2003), Characteristics of a tropospheric ozone profile and implications for the origin of ozone over subtropical China in the spring of 2001, *J. Geophys. Res.*, *108*(D20), 8800, doi:10.1029/2003JD003427.

Chang, W., and H. Liao (2009), Anthropogenic direct radiative forcing of tropospheric ozone and aerosols from 1850 to 2000 estimated with IPCC AR5 emissions inventories, *Atmos. Oceanic Sci. Lett.*, *2*(4), 201–207.

Chang, W., H. Liao, and H. Wang (2009), Climate responses to direct radiative forcing of anthropogenic aerosols, tropospheric ozone, and long-lived greenhouse gases in eastern China over 1951–2000, *Adv. Atmos. Sci.*, *26*, 748–762, doi:10.1007/s00376-009-9032-4.

Chen, D., Y. Wang, M. B. McElroy, K. He, R. M. Yantosca, and P. Le Sager (2009), Regional CO pollution and export in China simulated by the high-resolution nested-grid GEOS-Chem model, *Atmos. Chem. Phys.*, *9*, 3825–3839, doi:10.5194/acp-9-3825-2009.

Cionni, I., V. Eyring, J. F. Lamarque, W. J. Randel, D. S. Stevenson, F. Wu, G. E. Bodeker, T. G. Shepherd, D. T. Shindell, and D. W. Waugh (2011), Ozone database in support of CMIP5 simulations: Results and corresponding radiative forcing, *Atmos. Chem. Phys.*, *11*, 11,267–11,292, doi:10.5194/acp-11-11267-2011.

Coleman, L., D. Martin, S. Varghese, S. G. Jennings, and C. D. O'Dowd (2013), Assessment of changing meteorology and emissions on air quality using a regional climate model: Impact on ozone, *Atmos. Environ.*, *69*, 198–210, doi:10.1016/j.atmosenv.2012.11.048.

Ding, A. J., T. Wang, V. Thouret, J. P. Cammas, and P. Nedelec (2008), Tropospheric ozone climatology over Beijing: Analysis of aircraft data from the MOZAIC program, *Atmos. Chem. Phys.*, *8*, 1–13, doi:10.5194/acp-8-1-2008.

Doherty, R. M., et al. (2013), Impacts of climate change on surface ozone and intercontinental ozone pollution: A multi-model study, *J. Geophys. Res. Atmos.*, *118*, 3744–3763, doi:10.1002/jgrd.50266.

Duan, Y., Y. Zhang, D. Wang, J. Xu, H. Wei, and H. Cui (2011), Spatial-temporal patterns analysis of ozone pollution in several cities of China [in Chinese], *Adm. Techn. Environ. Monit.*, *23*, 34–39.

Eyring, V., et al. (2013), Long-term ozone changes and associated climate impacts in CMIP5 simulations, *J. Geophys. Res. Atmos.*, *118*, 5029–5060, doi:10.1002/jgrd.50316.

Fairlie, T. D., D. J. Jacob, and R. J. Park (2007), The impact of transpacific transport of mineral dust in the United States, *Atmos. Environ.*, *41*, 1251–1266, doi:10.1016/j.atmosenv.2006.09.048.

Fann, N., A. D. Lamson, S. C. Anenberg, K. Wesson, D. Risley, and B. J. Hubbell (2012), Estimating the national public health burden associated with exposure to ambient $PM_{2.5}$ and ozone, *Risk Anal.*, *32*, 81–95, doi:10.1111/j.1539-6924.2011.01630.x.

Feng, Z., and K. Kobayashi (2009), Assessing the impacts of current and future concentrations of surface ozone on crop yield with meta-analysis, *Atmos. Environ.*, *43*(8), 1510–1519, doi:10.1016/j.atmosenv.2008.11.033.

Fiore, A. M., et al. (2012), Global air quality and climate, *Chem. Soc. Rev.*, *41*, 6663–6683, doi:10.1039/c2cs35095e.

Fuentes, J. D., H. R. Tai, and J. Zenker (2013), Ozone impedes the ability of a herbivore to find its host, *Environ. Res. Lett.*, *8*, 014048, doi:10.1088/1748-9326/8/1/014048.

Gao, J., B. Zhu, D. Wang, and F. Wang (2012), The variation of air pollutants and the impact of long-range transport in the northern suburb of Nanjing [in Chinese], *Acta Sci. Circumstantiae*, *32*(5), 1149–1159.

Gao, Y., J. S. Fu, J. B. Drake, J. F. Lamarque, and Y. Liu (2013), The impact of emission and climate change on ozone in the United States under representative concentration pathways (RCPs), *Atmos. Chem. Phys.*, *13*, 9607–9621, doi:10.5194/acp-13-9607-2013.

Guenther, A., T. Karl, P. Harley, C. Wiedinmyer, P. I. Palmer, and C. Geron (2006), Estimates of global terrestrial isoprene emissions using MEGAN (Model of Emissions of Gases and Aerosols from Nature), *Atmos. Chem. Phys.*, *6*, 3181–3210, doi:10.5194/acp-6-3181-2006.

Hansen, J., et al. (2007), Climate simulations for 1880–2003 with GISS modelE, *Clim. Dyn.*, *29*, 661–696, doi:10.1007/s00382-007-0255-8.

Hauglustaine, D. A., and G. P. Brasseur (2001), Evolution of tropospheric ozone under anthropogenic activities and associated radiative forcing of climate, *J. Geophys. Res.*, *106*, 32,337–32,360, doi:10.1029/2001JD900175.

He, K. B. (2012), Multi-resolution Emission Inventory for China (MEIC): Model framework and 1990–2010 anthropogenic emissions, paper presented at 12th International Global Atmospheric Chemistry Conference, Beijing, China.

He, Y. J., I. Uno, Z. F. Wang, P. Pochanart, J. Li, and H. Akimoto (2008), Significant impact of the East Asia monsoon on ozone seasonal behavior in the boundary layer of Eastern China and the west Pacific region, *Atmos. Chem. Phys.*, *8*, 7543–7555, doi:10.5194/acp-8-7543-2008.

Intergovernmental Panel on Climate Change (IPCC) (2013), *Climate Change 2013: The Physical Science Basis. Working Group I Contribution to the Fifth Assessment Report of the Intergovernmental Panel on Climate Change*, Cambridge Univ. Press, Cambridge, U. K.

Jacob, D. J., and D. A. Winner (2009), Effect of climate change on air quality, *Atmos. Environ.*, *43*, 51–63, doi:10.1016/j.atmosenv.2008.09.051.

Jhun, I., N. Fann, A. Zanobetti, and B. Hubbell (2014), Effect modification of ozone-related mortality risks by temperature in 97 US cities, *Environ. Int.*, *73*, 128–134, doi:10.1016/j.envint.2014.07.009.

Juda-Rezler, K., et al. (2012), Modelling the effects of climate change on air quality over Central and Eastern Europe: Concept, evaluation and projections, *Clim. Res.*, *53*, 179–203, doi:10.3354/cr01072.

Katragkou, E., P. Zanis, I. Kioutsioukis, I. Tegoulias, D. Melas, B. C. Krüger, and E. Coppola (2011), Future climate change impacts on summer surface ozone from regional climate air quality simulations over Europe, *J. Geophys. Res.*, *116*, D22307, doi:10.1029/2011JD015899.
Kawase, H., T. Nagashima, K. Sudo, and T. Nozawa (2011), Future changes in tropospheric ozone under Representative Concentration Pathways (RCPs), *Geophys. Res. Lett.*, *38*, L05801, doi:10.1029/2010GL046402.
Kelly, J., P. A. Makar, and D. A. Plummer (2012), Projections of mid-century summer air-quality for North America: Effects of changes in climate and precursor emissions, *Atmos. Chem. Phys.*, *12*(12), 5367–5390, doi:10.5194/acp-12-5367-2012.
Kim, M. J., R. J. Park, C. Ho, J. H. Woo, K. C. Choi, C. K. Song, and J. B. Lee (2014), Future ozone and oxidants change under the RCP scenarios, *Atmos. Environ.*, *101*, 103–115, doi:10.1016/j.atmosenv.2014.11.016.
Kurokawa, J., T. Ohara, I. Uno, M. Hayasaki, and H. Tanimoto (2009), Influence of meteorological variability on interannual variations of springtime boundary layer ozone over Japan during 1981–2005, *Atmos. Chem. Phys.*, *9*, 6287–6304, doi:10.5194/acp-9-6287-2009.
Lam, S. H. M., S. M. Saunders, H. Guo, Z. H. Ling, F. Jiang, X. M. Wang, and T. J. Wang (2013), Modelling VOC source impacts on high ozone episode days observed at a mountain summit in Hong Kong under the influence of mountain-valley breezes, *Atmos. Environ.*, *81*, 166–176, doi:10.1016/j.atmosenv.2013.08.060.
Langner, J., et al. (2012), A multi-model study of impacts of climate change on surface ozone in Europe, *Atmos. Chem. Phys.*, *12*, 10,423–10,440, doi:10.5194/acp-12-10423-2012.
Lapina, K., D. K. Henze, J. B. Milford, C. Cuvelier, and M. Seltzer (2015), Implications of RCP emissions for future changes in vegetative exposure to ozone in the western U.S, *Geophys. Res. Lett.*, *42*, 4190–4198, doi:10.1002/2015GL063529.
Lauwaet, D., et al. (2014), The effect of climate change and emission scenarios on ozone concentrations over Belgium: A high resolution model study for policy support, *Atmos. Chem. Phys.*, *14*, 5893–5904, doi:10.5194/acp-14-5893-2014.
Lee, J. B., et al. (2015), Projections of summertime ozone concentration over East Asia under multiple IPCC SRES emission scenarios, *Atmos. Environ.*, *106*, 335–346, doi:10.1016/j.atmosenv.2015.02.019.
Lei, Y., Q. Zhang, K. B. He, and D. G. Streets (2011), Primary anthropogenic aerosol emission trends for China, 1990–2005, *Atmos. Chem. Phys.*, *11*, 931–954, doi:10.5194/acp-11-931-2011.
Li, Y., C. Zhao, Y. Fang, and H. Yu (2007), Analysis of distribution and seasonal change of tropospheric ozone residual in recent 20 years using satellite data [in Chinese], *J. Appl. Meteorol. Sci.*, *18*(2), 181–186.
Liao, H., W. T. Chen, and J. H. Seinfeld (2006), Role of climate change in global predictions of future tropospheric ozone and aerosols, *J. Geophys. Res.*, *111*, D12304, doi:10.1029/2005JD006852.
Lin, M., T. Holloway, T. Oki, D. G. Streets, and A. Richter (2009), Multi-scale model analysis of boundary layer ozone over East Asia, *Atmos. Chem. Phys.*, *9*, 3277–3301, doi:10.5194/acp-9-3277-2009.
Lin, W., X. Xu, L. Wang, S. Yang, Y. Lin, Z. Zhao, J. Li, and Q. Chen (2010), On-line measurement of reactive gases at Akedala regional atmosphere background station [in Chinese], *Meteorol. Sci. Technol.*, *38*(6), 661–667.
Liu, Q., K. S. Lam, F. Jiang, T. J. Wang, M. Xie, B. L. Zhuang, and X. Y. Jiang (2013), A numerical study of the impact of climate and emission changes on surface ozone over South China in autumn time in 2000–2050, *Atmos. Environ.*, *76*, 227–237, doi:10.1016/j.atmosenv.2013.01.030.
Liu, X., et al. (2006), First directly retrieved global distribution of tropospheric column ozone from GOME: Comparison with the GEOS-CHEM model, *J. Geophys. Res.*, *111*, D02308, doi:10.1029/2005JD006564.
Lou, S., B. Zhu and H. Liao (2010), Impacts of O_3 precursor on surface O_3 concentration over China [in Chinese], *Trans. Atmos. Sci.*, *33*, 451–459.
Lou, S., H. Liao, and B. Zhu (2014), Impacts of aerosols on surface-layer ozone concentrations in China through heterogeneous reactions and changes in photolysis rates, *Atmos. Environ.*, *85*, 123–138, doi:10.1016/j.atmosenv.2013.12.004.
Ma, J. (2011), Effects of vertical transport on surface O_3 in Shangri-la and DangXiong [in Chinese], M. S. thesis, Chinese Academy of Meteorological Sciences, Beijing, China.
Mao, J., F. Paulot, D. J. Jacob, R. C. Cohen, J. D. Crounse, P. O. Wennberg, C. A. Keller, R. C. Hudman, M. P. Barkley, and L. W. Horowitz (2013), Ozone and organic nitrates over the eastern United States: Sensitivity to isoprene chemistry, *J. Geophys. Res. Atmos.*, *118*, 11,256–11,268, doi:10.1002/jgrd.50817.
McLinden, C. A., S. C. Olsen, B. Hannegan, O. Wild, M. J. Prather, and J. Sundet (2000), Stratospheric ozone in 3-D models: A simple chemistry and the cross-tropopause flux, *J. Geophys. Res.*, *105*, 14,653–14,665, doi:10.1029/2000JD900124.
Moss, R. H., et al. (2010), The next generation of scenarios for climate change research and assessment, *Nature*, *463*, 747–756, doi:10.1038/nature08823.
Murazaki, K., and P. Hess (2006), How does climate change contribute to surface ozone change over the United States?, *J. Geophys. Res.*, *111*, D05301, doi:10.1029/2005JD005873.
Murray, L. T., D. J. Jacob, J. A. Logan, R. C. Hudman, and W. J. Koshak (2012), Optimized regional and interannual variability of lightning in a global chemical transport model constrained by LIS/OTD satellite data, *J. Geophys. Res.*, *117*, D20307, doi:10.1029/2012JD017934.
Park, R. J., D. J. Jacob, M. Chin and R. V. Martin (2003), Sources of carbonaceous aerosols over the United States and implications for natural visibility, *J. Geophys. Res.*, *108*(D12), 4355, doi:10.1029/2002JD003190.
Park, R. J., D. J. Jacob, B. D. Field, R. M. Yantosca, and M. Chin (2004), Natural and transboundary pollution influences on sulfate-nitrate-ammonium aerosols in the United States: Implications for policy, *J. Geophys. Res.*, *109*, D15204, doi:10.1029/2003JD004473.
Pfister, G. G., S. Walters, J. F. Lamarque, J. Fast, M. C. Barth, J. Wong, J. Done, G. Holland, and C. L. Bruyère (2014), Projections of future summertime ozone over the U.S., *J. Geophys. Res. Atmos.*, *119*, 5559–5582, doi:10.1002/2013JD020932.
Pye, H. O. T., H. Liao, S. Wu, L. J. Mickley, D. J. Jacob, D. K. Henze, and J. H. Seinfeld (2009), Effect of changes in climate and emissions on future sulfate-nitrate-ammonium aerosol levels in the United States, *J. Geophys. Res.*, *114*, D01205, doi:10.1029/2008JD010701.
Racherla, P. N., and P. J. Adams (2006), Sensitivity of global tropospheric ozone and fine particulate matter concentrations to climate change, *J. Geophys. Res.*, *111*, D24103, doi:10.1029/2005JD006939.
Racherla, P. N., and P. J. Adams (2009), U.S. ozone air quality under changing climate and anthropogenic emissions, *Environ. Sci. Technol.*, *43*, 571–577, doi:10.1021/es800854f.
Rasmussen, D. J., A. M. Fiore, V. Naik, L. W. Horowitz, S. J. McGinnis, and M. G. Schultz (2012), Surface ozone-temperature relationships in the eastern US: A monthly climatology for evaluating chemistry-climate models, *Atmos. Environ.*, *47*, 142–153, doi:10.1016/j.atmosenv.2011.11.021.
Sauvage, B., R. V. Martin, A. van Donkelaar, X. Liu, K. Chance, L. Jaeglé, P. I. Palmer, S. Wu, and T. M. Fu (2007), Remote sensed and in situ constraints on processes affecting tropical tropospheric ozone, *Atmos. Chem. Phys.*, *7*, 815–838, doi:10.5194/acp-7-815-2007.
Shindell, D. T., G. Faluvegi, and N. Bell (2003), Preindustrial-to-present-day radiative forcing by tropospheric ozone from improved simulations with the GISS chemistry-climate GCM, *Atmos. Chem. Phys.*, *3*, 1675–1702, doi:10.5194/acp-3-1675-2003.
Stevenson, D. S., et al. (2013), Tropospheric ozone changes, radiative forcing and attribution to emissions in the Atmospheric Chemistry and Climate Model Intercomparison Project (ACCMIP), *Atmos. Chem. Phys.*, *13*, 3063–3085, doi:10.5194/acp-13-3063-2013.

Su, M., Y. Lin, X. Fan, L. Peng, and C. Zhao (2012), Impacts of global emissions of CO, NO_x, and CH_4 on China tropospheric hydroxyl free radicals, *Adv. Atmos. Sci.*, *29*, 838–854, doi:10.1007/s00376-012-1229-2.

Sudo, K., M. Takahashi, and H. Akimoto (2003), Future changes in stratosphere-troposphere exchange and their impacts on future tropospheric ozone simulations, *Geophys. Res. Lett.*, *30*(24), 2256, doi:10.1029/2003GL018526.

Szopa, S., et al. (2013), Aerosol and ozone changes as forcing for climate evolution between 1850 and 2100, *Clim. Dyn.*, *40*, 2223–2250, doi:10.1007/s00382-012-1408-y.

Tagaris, E., K. Manomaiphiboon, K.-J. Liao, L. R. Leung, J.-H. Woo, S. He, P. Amar, and A. G. Russell (2007), Impacts of global climate change and emissions on regional ozone and fine particulate matter concentrations over the United States, *J. Geophys. Res.*, *112*, D14312, doi:10.1029/2006JD008262.

Tai, A. P. K., M. Val Martin, and C. L. Heald (2014), Threat to future global food security from climate change and ozone air pollution, *Nat. Clim. Change*, *4*, 817–821, doi:10.1038/nclimate2317.

Tang, H., G. Liu, J. Zhu, Y. Han, and K. Kobayashi (2013), Seasonal variations in surface ozone as influenced by Asian summer monsoon and biomass burning in agricultural fields of the northern Yangtze River Delta, *Atmos. Res.*, *122*, 67–76, doi:10.1016/j.atmosres.2012.10.030.

Taylor, K. E., R. J. Stouffer, and G. A. Meehl (2012), An overview of CMIP5 and the experiment design, *Bull. Am. Meteorol. Soc.*, *93*, 485–498, doi:10.1175/bams-d-11-00094.1.

Val Martin, M., C. L. Heald, J.-F. Lamarque, S. Tilmes, L. K. Emmons, and B. A. Schichtel (2015), How emissions, climate, and land use change will impact mid-century air quality over the United States: A focus on effects at national parks, *Atmos. Chem. Phys.*, *15*, 2805–2823, doi:10.5194/acp-15-2805-2015.

Voulgarakis, A., et al. (2013), Analysis of present day and future OH and methane lifetime in the ACCMIP simulations, *Atmos. Chem. Phys.*, *13*, 2563–2587, doi:10.5194/acp-13-2563-2013.

Wang, T., X. L. Wei, A. J. Ding, C. N. Poon, K. S. Lam, Y. S. Li, L. Y. Chan, and M. Anson (2009), Increasing surface ozone concentrations in the background atmosphere of Southern China, 1994–2007, *Atmos. Chem. Phys.*, *9*, 6217–6227, doi:10.5194/acp-9-6217-2009.

Wang, T., et al. (2010), Air quality during the 2008 Beijing Olympics: Secondary pollutants and regional impact, *Atmos. Chem. Phys.*, *10*, 7603–7615, doi:10.5194/acp-10-7603-2010.

Wang, W. G., J. Wu, H. N. Liu, S. C. Guo, X. M. Chen, and Y. Luo (2005), Researches on the influence of pollution emission on tropospheric ozone variation and radiation over China and its adjacent area [in Chinese], *Chin. J. Atmos. Sci.*, *29*(5), 734–746.

Wang, Y., M. B. McElroy, J. W. Munger, J. Hao, H. Ma, C. P. Nielsen, and Y. Chen (2008), Variations of O_3 and CO in summertime at a rural site near Beijing, *Atmos. Chem. Phys.*, *8*, 6355–6363, doi:10.5194/acp-8-6355-2008.

Wang, Y., Y. Zhang, J. Hao, and M. Luo (2011), Seasonal and spatial variability of surface ozone over China: Contributions from background and domestic pollution, *Atmos. Chem. Phys.*, *11*(7), 3511–3525, doi:10.5194/acp-11-3511-2011.

Wang, Y., L. Shen, S. Wu, L. Mickley, J. He, and J. Hao (2013), Sensitivity of surface ozone over China to 2000–2050 global changes of climate and emissions, *Atmos. Environ.*, *75*, 374–382, doi:10.1016/j.atmosenv.2013.04.045.

Wei, H., and Y. Zheng (2006), Analysis of the temporal and spatial distributions of the total ozone over China [in Chinese], *J. Nanjing Inst. Meteorol.*, *29*(3), 390–395.

Wild, O., and H. Akimoto (2001), Intercontinental transport of ozone and its precursors in a three-dimensional global CTM, *J. Geophys. Res.*, *106*(D21), 27,729–27,744, doi:10.1029/2000JD000123.

Wild, O., et al. (2012), Modelling future changes in surface ozone: A parameterized approach, *Atmos. Chem. Phys.*, *12*, 2037–2054, doi:10.5194/acp-12-2037-2012.

Wilkinson, S., G. Mills, R. Illidge, and W. J. Davies (2011), How is ozone pollution reducing our food supply?, *J. Exp. Bot.*, *63*, 527–536, doi:10.1093/jxb/err317.

Wu, J., W. M. Jiang, H. N. Liu, and J. P. Tang (2002), Using regional climate model and atmosphere chemical model to model regional climate and ozone in troposphere over China [in Chinese], *J. Nanjing Univ.*, *38*, 572–582.

Wu, S., L. J. Mickley, D. J. Jacob, D. Rind, and D. G. Streets (2008a), Effects of 2000–2050 changes in climate and emissions on global tropospheric ozone and the policy-relevant background surface ozone in the United States, *J. Geophys. Res.*, *113*, D18312, doi:10.1029/2007JD009639.

Wu, S., L. J. Mickley, E. M. Leibensperger, D. J. Jacob, D. Rind, and D. G. Streets (2008b), Effects of 2000–2050 global change on ozone air quality in the United States, *J. Geophys. Res.*, *113*, D06302, doi:10.1029/2007JD008917.

Xie, F., W. S. Tian, J. P. Li, J. K. Zhang, and L. Shang (2013), Effects of future increase in methane emission on the stratospheric water vapor and global ozone [in Chinese], *Acta. Meteorol. Sin.*, *71*, 555–567, doi:10.11676/qxxb2013.049.

Yan, P., X. Li, C. Luo, X. Xu, R. Xiang, G. Ding, J. Tang, M. Wang, and X. Yu (1997), Observational analysis of surface O_3, NO_x and SO_2 in China [in Chinese], *J. Appl. Meteorol.*, *8*(1), 53–61.

Yang, C., H. Yang, S. Guo, Z. Wang, X. Xu, X. Duan, and H. Kan (2012), Alternative ozone metrics and daily mortality in Suzhou: The China Air Pollution and Health Effects Study (CAPES), *Sci. Total Environ.*, *426*, 83–89, doi:10.1016/j.scitotenv.2012.03.036.

Yang, Y., and H. Gao (2008), Dynamics of ozone and its precursors in the atmosphere and their pollution characteristics in Qingdao, Shandong province [in Chinese], *J. Meteorol. Environ.*, *24*(2), 1–5.

Yang, Y., H. Liao, and J. Li (2014), Impacts of the East Asian summer monsoon on interannual variations of summertime surface-layer ozone concentrations over China, *Atmos. Chem. Phys.*, *14*, 6867–6879, doi:10.5194/acp-14-6867-2014.

Yienger, J. J., and H. Levy (1995), Empirical-model of global soil-biogenic NO_x emissions, *J. Geophys. Res.*, *100*, 11,447–11,464, doi:10.1029/95JD00370.

Young, P. J., et al. (2013a), Preindustrial to end 21st century projections of tropospheric ozone from the Atmospheric Chemistry and Climate Model Intercomparison Project (ACCMIP), *Atmos. Chem. Phys.*, *13*, 2063–2090, doi:10.5194/acp-13-2063-2013.

Young, P. J., et al. (2013b), Corrigendum to "Pre-industrial to end 21st century projections of tropospheric ozone from the Atmospheric Chemistry and Climate Model Intercomparison Project (ACCMIP)" published in Atmos. Chem. Phys., 13, 2063–2090, 2013, *Atmos. Chem. Phys.*, *13*, 5401–5402, doi:10.5194/acp-13-5401-2013.

Yue, X., and N. Unger (2014), Ozone vegetation damage effects on gross primary productivity in the United States, *Atmos. Chem. Phys.*, *14*, 9137–9153, doi:10.5194/acp-14-9137-2014.

Zhang, L., D. J. Jacob, X. Liu, J. A. Logan, K. Chance, A. Eldering, and B. R. Bojkov (2010), Intercomparison methods for satellite measurements of atmospheric composition: Application to tropospheric ozone from TES and OMI, *Atmos. Chem. Phys.*, *10*, 4725–4739, doi:10.5194/acp-10-4725-2010.

Zhang, Q., et al. (2007), NO_x emission trends for China, 1995–2004: The view from the ground and the view from space, *J. Geophys. Res.*, *112*, D22306, doi:10.1029/2007JD008684.

Zhang, Q., et al. (2009), Asian emissions in 2006 for the NASA INTEX-B mission, *Atmos. Chem. Phys.*, *9*, 5131–5153, doi:10.5194/acp-9-5131-2009.

Zhang, Q., B. Yuan, M. Shao, X. Wang, S. Lu, K. Lu, M. Wang, L. Chen, C. Chang, and S. Liu (2014), Variations of ground-level O_3 and its precursors in Beijing in summertime between 2005 and 2011, *Atmos. Chem. Phys.*, *14*, 6089–6101, doi:10.5194/acp-14-6089-2014.

Zhao, C., Y. Wang, Q. Yang, R. Fu, D. Cunnold, and Y. Choi (2010), Impact of East Asian summer monsoon on the air quality over China: View from space, *J. Geophys. Res.*, *115*, D09301, doi:10.1029/2009JD012745.

Zhu, B., T. Wang, and D. Ni (2004), Photochemical ozone and characteristics of its precursors in boundary layer of Lin'an, a rural/agricultural site of eastern China during autumn 1999 [in Chinese], *J. Nanjing Inst. Meteorol.*, *27*, 185–192, doi:10.13878/j.cnki.dqkxxb.2004.02.006.

Zhu, T., W. Lin, Y. Song, X. Cai, H. Zou, L. Kang, L. Zhou, and H. Akimoto (2006), Downward transport of ozone-rich air near Mt. Everest, *Geophys. Res. Lett.*, *33*, L23809, doi:10.1029/2006GL027726.